NASA CONTRACTOR REPORT 166473

Passive Orbital Disconnect Strut (PODS III), Structural and Thermal Test Program

R.T. Parmley

CONTRACT NAS2-10848
March 1983

NASA

NASA CONTRACTOR REPORT 166473

Passive Orbital Disconnect Strut (PODS III), Structural and Thermal Test Program

R.T. Parmley
Lockheed Missiles & Space Company
Palo Alto, CA 94304

Prepared for
Ames Research Center
Under Contract NAS2-10848

National Aeronautics and
Space Administration

Ames Research Center
Moffett Field, California 94035

FOREWORD

This work was conducted for the National Aeronautics and Space Administration through the AMES Research Center, Moffett Field, California, Dr. Peter Kittel, Program Manager.

The Lockheed Palo Alto Research Laboratory conducted the program within the Cryogenic Technology Group of the Materials Sciences Laboratory. Key individuals who contributed to the success of this program and their contributions are as follows:

Ed Cavey	-	Designed the PODS-III test article
R. Dammann	-	Assembled and checked out the thermal test article, test instrumentation and controls
Alan Holmes	-	Supervised the structural tests
Carol Jernberg	-	Assembled and checked out the thermal test setup
Dr. P. Kittel	-	Calculated the variation in heat rate as a function of the change in the RMS cross sectional area of the fiberglass tube
J. Skogh		Performed the structural analyses

R. T. Parmley
Principal Investigator

CONTENTS

CONTENTS (Cont'd)

ILLUSTRATIONS

ILLUSTRATIONS (Cont.)

TABLES

Section 1
INTRODUCTION AND SUMMARY

1.1 INTRODUCTION

A prior study (Ref. 1) has shown that the weight of a three-year lifetime superfluid helium dewar is cut in half if passive orbital disconnect strut (PODS) supports are used in place of nondisconnect, state-of-the-art, fiberglass tension-band supports. The objective of this program is to design, build, and test structurally (down to 78 K) and thermally (down to 4 K) an advanced concept of this PODS support (Mark III). The test data are then compared with the strut's predicted performance to verify the projected improvement in dewar performance.

1.2 SUMMARY OF PROGRAM TASKS

A detailed design is performed on the cold end (PODS-III) portion of the strut. Structural analysis of the thin-wall fiberglass tube allows selection of the optimum winding angle and tube dimensions.

Structural tests on the thin-wall fiberglass tube measure both the tension and compression modulus at ambient and LN_2 temperatures, the radial deflection versus side load, and the ultimate compression strength of the tube at LN_2 temperature. The thermal expansion of the fiberglass tube plus Invar is also measured down to 78 K. The axial gap at the wedge portion of the stem is set based on these data. The PODS-III test article parts are fabricated and assembled using a detailed assembly procedure.

An LN_2 guarded helium dewar test setup is designed, fabricated, assembled, and leak checked. A thermal link assembly is fabricated; the test article is mounted on the thermal link. The instrumented test article/thermal link subassembly is then installed on the helium tank inside a cylindrical cavity. The dewar is evacuated and the LN_2 guard plus helium tank are filled. The thermal link is calibrated by measuring the ΔT between two carbon temperature sensors and plotting the ΔT versus the heater power. To measure the heat rate through the PODS-III, the body temperature is raised in steps to approximately 6, 10, 20, 30, and 40 K. The heat leak (ΔT in the thermal link) is measured at each point. This temperature range covers the predicted ground hold and orbit temperatures for vapor-cooled supports. The test results are then compared with heat leak values predicted before the tests began. Side load, axial compression load, and tension load tests conclude the test program.

Section 2
PODS-III DESIGN CONCEPT

The PODS-III support concept is shown in Fig. 1. A minimum of six struts (three pairs) are required to support a cryogen tank. (Six struts provide a statically determinate support system.) As the tank diameter changes due to cooldown or pressurization, the angled pinned end struts are free to move in and out as the tank moves up or down slightly a value of H. The same adjustment occurs automatically as the vacuum shell changes diameter in orbit due to temperature changes.

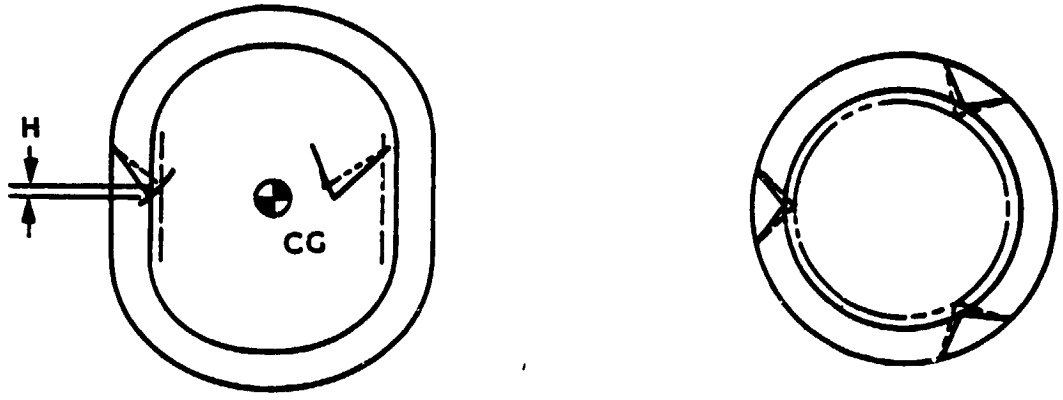

The warm end of the strut provides a length adjustment feature. The threads on the rod-end fitting and length adjustment are a different pitch; consequently, by rotating the adjustment hex, precise length adjustments can be made during strut installation without rotating the strut.

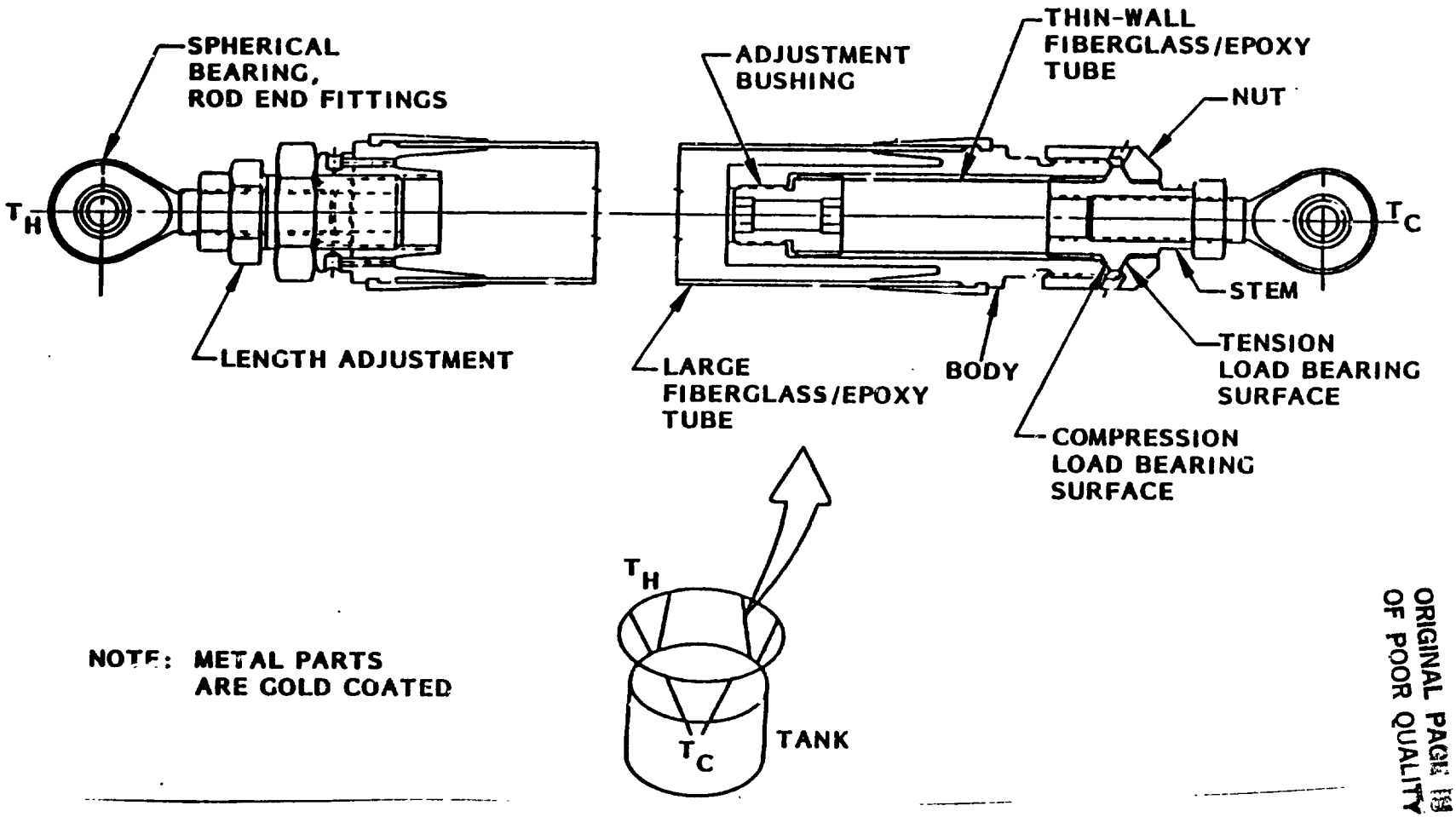

Fig. 1 PODS-III Support Concept

The cold end of the strut provides the passive orbital disconnect feature. The cold rod-end fitting/stem is connected to the body by a thin-wall fiberglass/epoxy tube and adjustment bushing. The conical stem load bearing surfaces are separated from the nut (tension) and body (compression) by an axial gap of ~ 0.099 mm (0.0039 in.) at operating temperature. (At ambient temperature, the gaps are set to take into account the differential shrinkage between the various parts.) During one-g thermal testing or orbital flight, the conical surfaces do not touch. Consequently, heat is transferred from the body to the thin-wall fiberglass tube/stem/rod end fitting subassembly by radiation and by conduction along the fiberglass tube. At the operating temperatures of the body (typically 15 to 20 K when vapor cooled) radiation heat transfer is negligible. Essentially all heat is transferred by conduction.

During launch, the g load elastically deforms the thin-wall fiberglass tube along its axis; the stem's conical shoulder rests hard on the body (compression) or nut (tension). The load path bypasses the thin-wall fiberglass tube. The major thermal resistance and load path during launch is now the large fiberglass tube. Upon achieving orbit, the stem's conical shoulder passively disconnects from the body or nut and the major thermal resistance is again the thin-wall fiberglass tube.

This design combines the desirable features of a thermal disconnect during ground hold and orbit with the high reliability of a completely passive design. Since the struts don't short out in one-g, the orbital performance of the struts can be demonstrated in one-g thermal qualification tests, and the ground hold heat leak is lower, both highly desirable features.

Section 3
PODS-III TEST ARTICLE

3.1 DESIGN

The design of the passive disconnect mechanism at the cold end of the strut is shown in Fig. 2. Detail drawings of the parts are shown in Figs. 3 through 8. The design is identical to that recommended for flight struts, with the following exceptions:

- Three holes are drilled in the end of the nut (Fig. 4) to measure the gap between the conical shoulder on the nut and stem (Fig. 3).
- The adjustment bushing threads (Fig. 6) and nut threads (Fig. 4) are not epoxy bonded for the thermal tests (to provide additional flexibility in conducting later tests).

During thermal tests, items 1, 2, 9, and 10 in Fig. 2 are not required.

Items shown below are connected together to form a single subassembly.

Item No.	
1	Rod end (Fig. 2)
2	Jam nut (Fig. 2)
3	Stem (Fig. 3)
8	Fiberglass tube (Fig. 8)
6	Adjustment bushing (Fig. 6)
7	Clamshells, 2 each (Fig. 7)

The rod-end fitting transmits pure axial loads down the strut; the spherical bearing in the rod end prevents side loads from occuring. The jam nut prevents the rod end from loosening in a dynamic launch environment. The mating conical surfaces between the stem (Fig. 3) and nut (Fig. 4) or body (Fig. 5) ensures that load is centered during launch, thus preventing premature buckling of the large fiberglass tube.

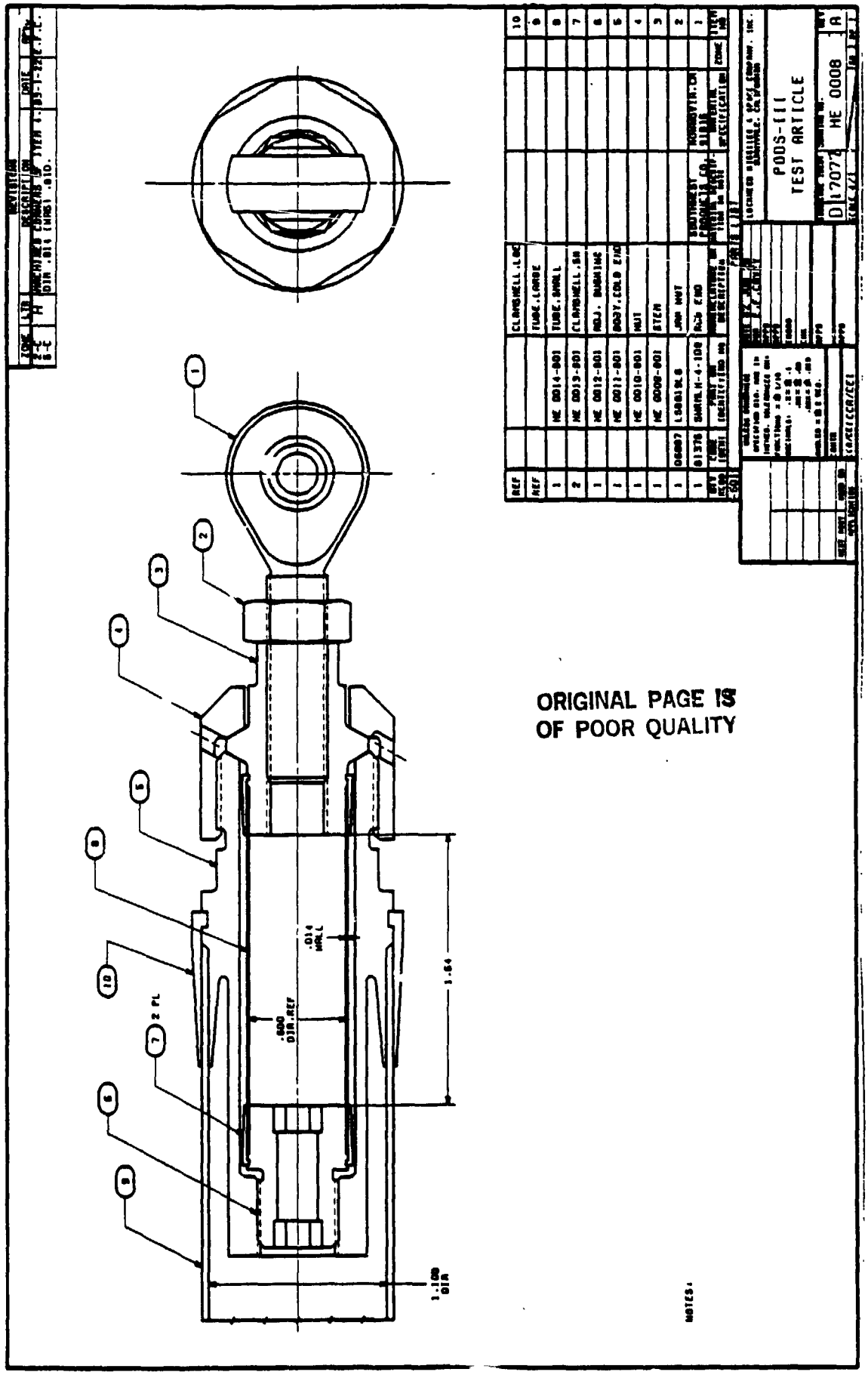

Fig. 2 PODS-III Test Article

ORIGINAL PAGE IS
OF POOR QUALITY

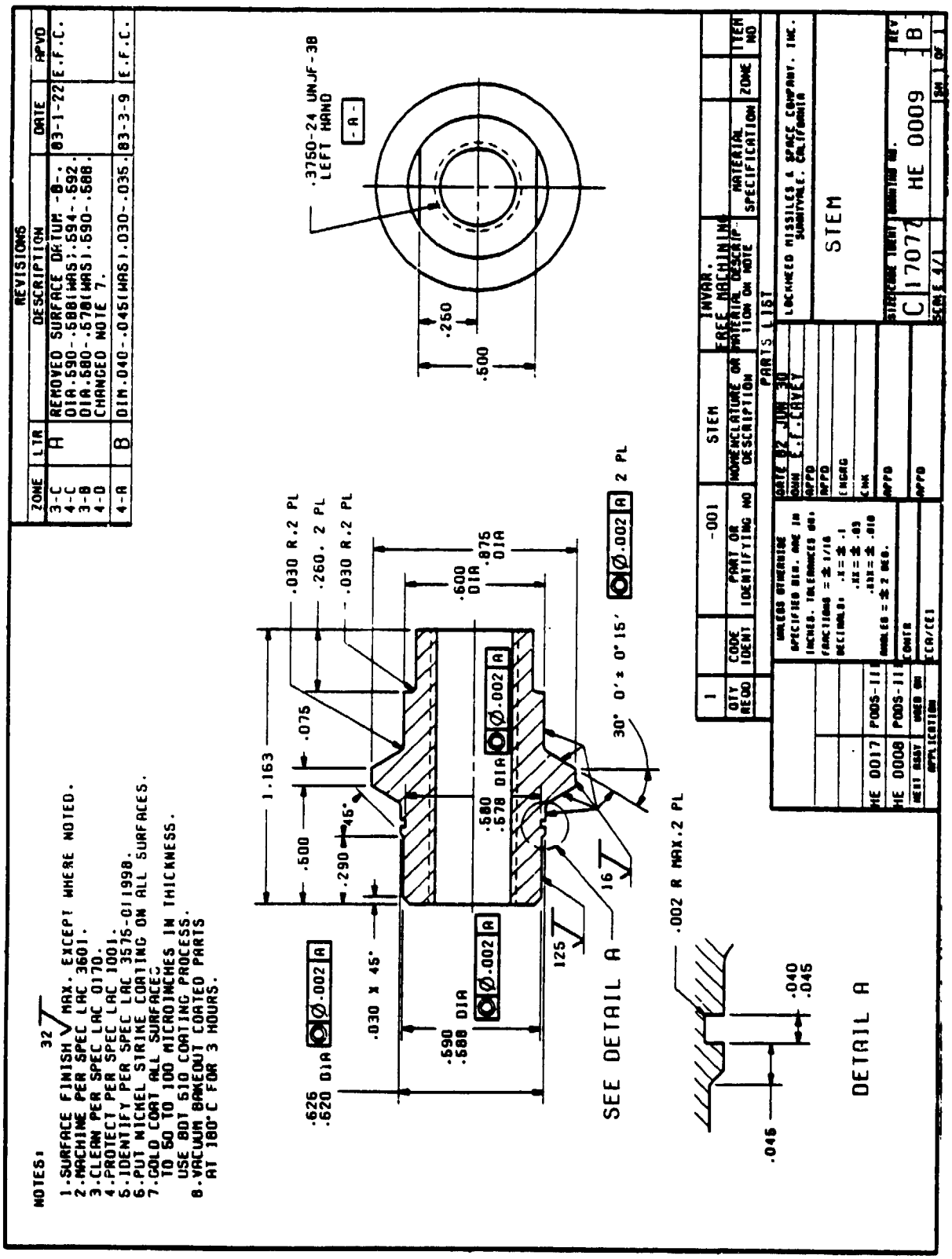

Fig. 3 Stem

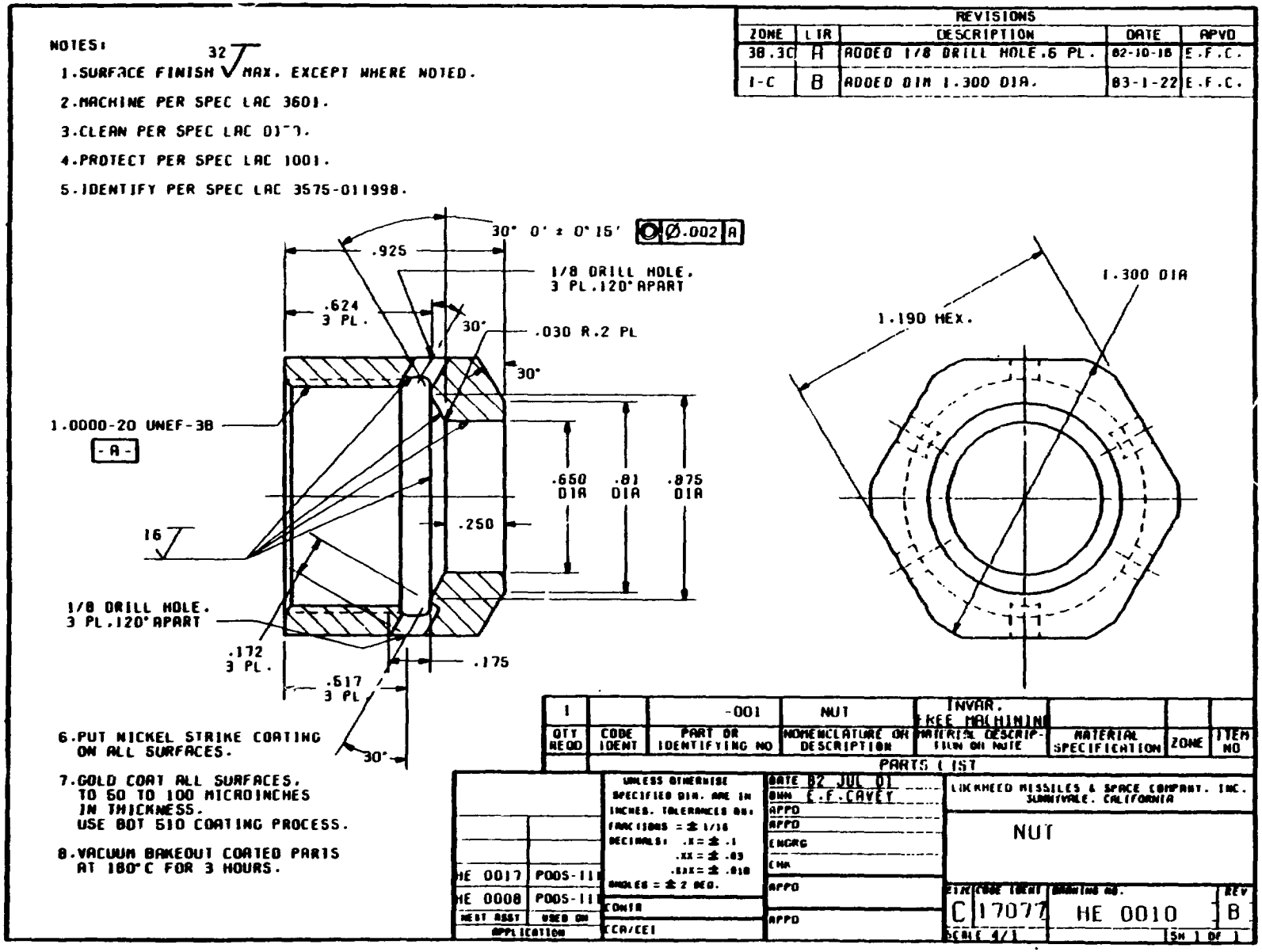

Fig. 4 Nut

ORIGINAL PAGE IS
OF POOR QUALITY

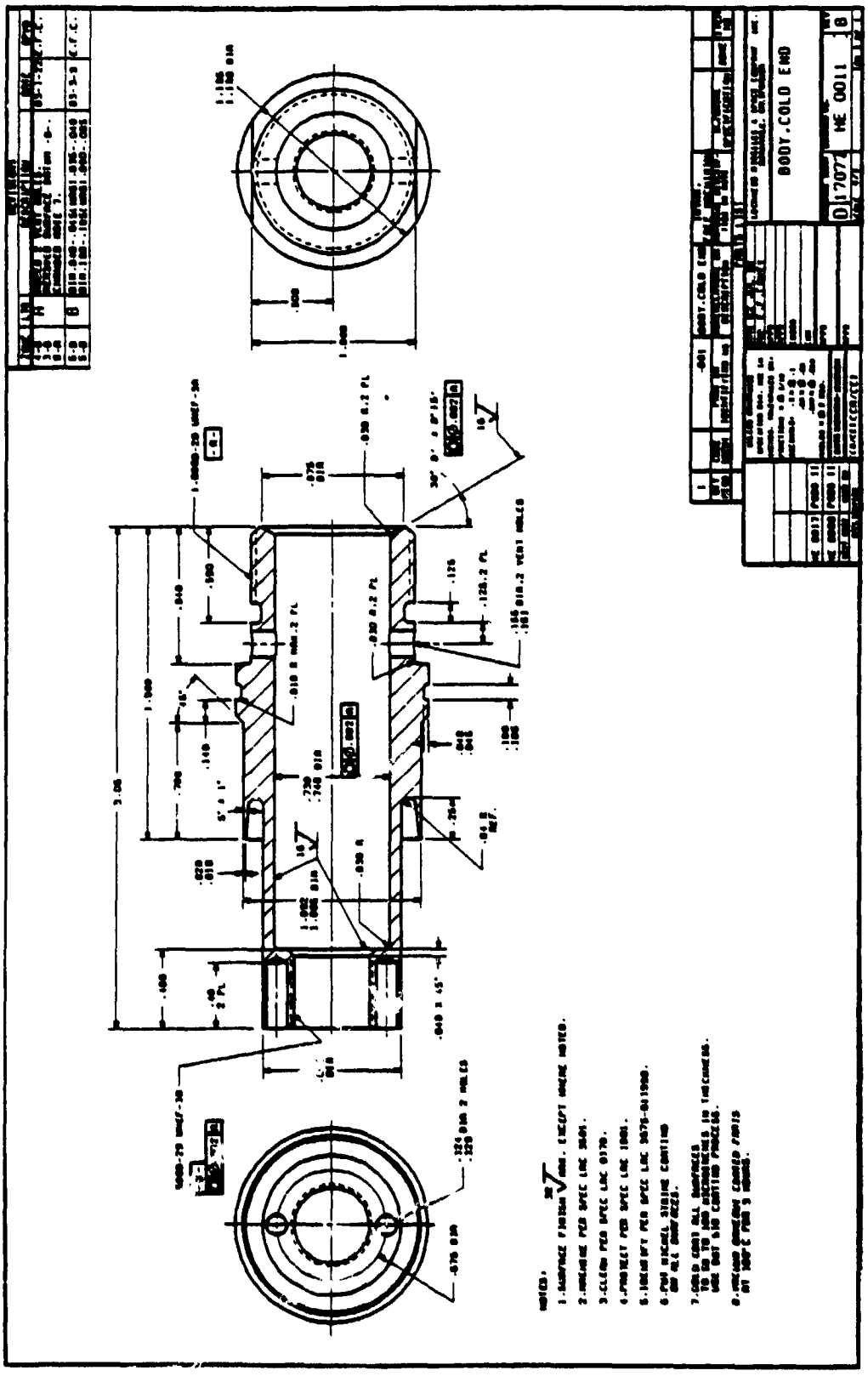

Fig. 5 Body

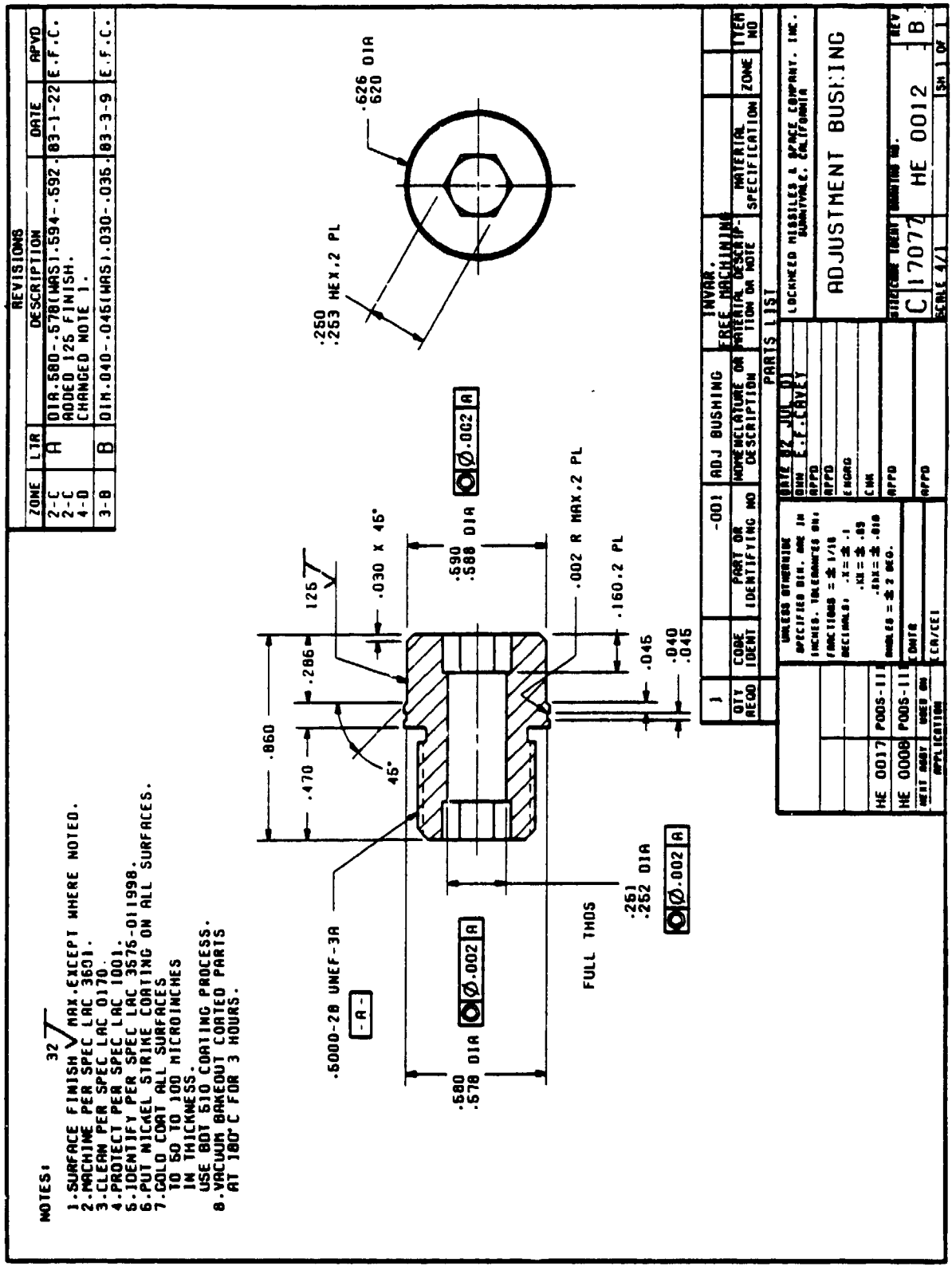

Fig. 6 Adjustment Bushing

NOTES:

1. SURFACE FINISH 32 √ MAX. EXCEPT WHERE NOTED.
2. MACHINE PER SPEC LAC 3601.
3. CLEAN PER SPEC LAC 0170.
4. PROTECT PER SPEC LAC 1001.
5. ONE -001 MAKES TWO MATCHED PARTS.
6. IDENTIFY PER SPEC LAC 3575-011990.BAG AS ONE PART.
7. PUT NICKEL STRIKE COATING ON ALL SURFACES.
8. GOLD COAT ALL SURFACES TO 50 TO 100 MICROINCHES IN THICKNESS. USE BDT 510 COATING PROCESS.
9. VACUUM BAKEOUT COATED PARTS AT 180°C FOR 3 HOURS.

REVISIONS				
ZONE	LTR	DESCRIPTION	DATE	APVD
3-C 2-C 2-C 3-C 3-B	A	DIA.690-.592(WAS).588-.590. DIA.642-.644(WAS).627-.630. DIA.670-.660(WAS).660-.650. ADDED 125 FINISH. REMOVED LIP AT THIN END.	83-1-22	E.F.C.

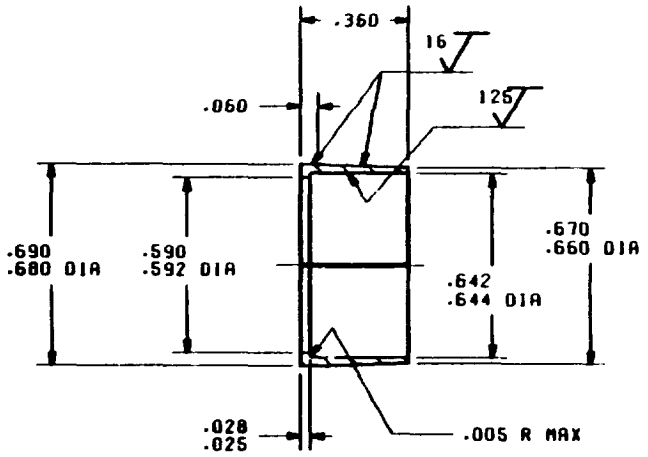

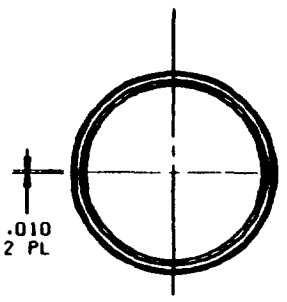

ORIGINAL PAGE IS OF POOR QUALITY

QTY REQD	CODE IDENT	PART OR IDENTIFYING NO	NOMENCLATURE OR DESCRIPTION	MATERIAL DESCRIPTION OR NOTE	MATERIAL SPECIFICATION	ZONE	ITEM NO
2		-001	CLAMSHELL	INVAR. FREE MACHINING			

PARTS LIST

HE 0017	PODS-II
HE 0008	PODS-II
NEXT ASSY	USED ON
APPLICATION	

UNLESS OTHERWISE SPECIFIED DIM. ARE IN INCHES. TOLERANCES ON: FRACTIONS = ± 1/16 DECIMALS: .X = ± .1, .XX = ± .03, .XXX = ± .010 ANGLES = ± 2 DEG.

CONTR XXXXXXXXXXXXX

CCA/CEI

DATE 82 JUL 06
DWN E.F.CAVEY
APPD
APPD
ENGRG
CHK
APPD
APPD

LOCKHEED MISSILES & SPACE COMPANY, INC. SUNNYVALE, CALIFORNIA

SMALL CLAMSHELL

SIZE	CODE IDENT	DRAWING NO.	REV
C	17077	HE 0013	A

SCALE 4/1 SH 1 OF 1

Fig. 7 Clamshell

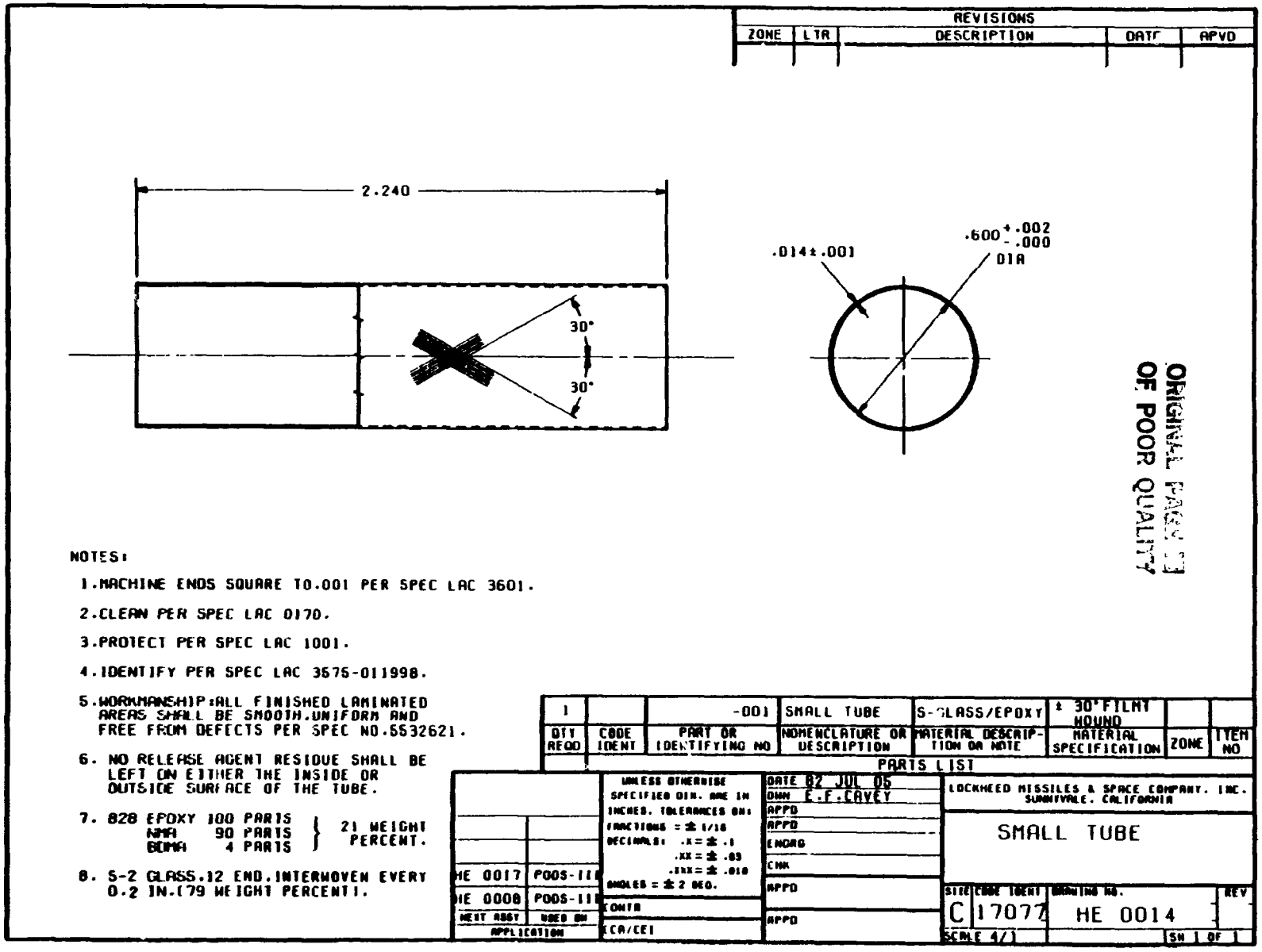

Fig. 8 Thin-Wall Fiberglass Tube

The thin-wall fiberglass tube (Fig. 8) is epoxy bonded to both the stem (Fig. 3) and adjustment bushing (Fig. 6). Split clamshells (Fig. 7) are bonded over the tube ends as an added precaution to ensure structural integrity. Four-mil glass beads in the epoxy maintain the bond line thickness. The internal hexes on both ends of the adjustment bushing (Fig. 6) allow final adjustment of the stem/body conical gap from either end. The center hole through the adjustment bushing (Fig. 6) vents the fiberglass tube during pumpdown and is used as a centering guide during fiberglass tube bonding.

The gap between the nut (Fig. 4) and stem (Fig. 3) conical surfaces is adjustable by screwing the nut on the body the desired amount. Flats on the stem (Fig. 3), body (Fig. 5), and nut (Fig. 4) allow the parts to be held with tools as the final gap adjustments are made. Six holes through the side of the nut (Fig. 4) allow shims to be used to set the gaps accurately. The faired design on the body (Fig. 5), where the large fiberglass tube is bonded, minimizes the stress buildup in this transition region.

3.2 STRUCTURAL ANALYSIS

Different parts of the PODS-III support are affected by the following design criteria:

CRITERIA	AFFECTS DESIGN OF
Launch Loads	• Large fiberglass/epoxy tube • Stem wedge area
Launch Resonance and Launch Thermal Resistance	• Large fiberglass/epoxy tube
Orbit Resonance, Orbit Thermal Resistance, and One-G Thermal Test Requirement	• Thin-wall fiberglass/epoxy tube and gap spacing

Note the launch requirements design the large fiberglass/epoxy tube, while orbit requirements and one-g thermal test requirements design the thin-wall fiberglass tube.

This feature is highly desirable as it allows the dimensions of each tube to be optimized separately. This optimizaton, performed on the PANDA-DEWAR program, considers the factors shown below.

		FIBERGLASS/EPOXY TUBE DIMENSIONAL RELATIONSHIPS		
	PROPERTY	Tube Radius	Wall Thickness	Length
STRUCTURAL	• Resonance	$\sqrt{R}$	$\sqrt{t}$	$\frac{1}{\sqrt{L}}$
	• Tensile Strength	R	t	-
	• Column Buckling Strength	R^3	t	$\frac{1}{L^2}$
	• Local Crippling Strength	$\frac{1}{R}$	t	-
	• Side Load Resistance	R^3	t	$\frac{1}{L^3}$
THERMAL	• Conduction Resistance	$\frac{1}{R}$	$\frac{1}{t}$	L
	• Radiation Resistance	$\frac{1}{R}$	-	$\frac{1}{t}$

It is desirable to have the highest value possible for each property shown: (1) resonance, (2) tensile strength, (3) column buckling strength, (4) local crippling strength, (5) side load capability, and (6) both conduction and radiation resistance. In order to maximize these properties, the fiberglass tube radius, wall thickness, and length relationships shown should be at their highest values. As usual, for most of the properties the structural requirement of a large radius, thick walled, short tube is in direct opposition to the thermal requiremnt of a small radius, thin walled, long tube. This is not true in all cases though; local crippling capability goes up as the radius goes down, and the radiation heat transfer goes down with shorter lengths (less radiating area).

For column buckling, increasing the radius proportionately increases the buckling strength faster than decreasing the length. Radiation resistance

increases when both the tube radius and length goes down. Resonance, side load, and conduction resistance values do not change when the changes in R and L are opposite and equal on a proportional basis.

The PANDA-DEWAR program previously optimized the large fiberglass/epoxy tubes dimensions [1] using the criteria discussed above, but not the thin wall tube dimensions, since the prior study was based on the earlier PODS-I design. The PANDA-DEWAR program will be modified later to include the PODS-III design. In lieu of using this program, the thin-wall tube dimensions were set based on the following criteria:

- Six struts must support 431 kg (950 lb) in one-g without shorting (same as Ref 1).
- The orbit reasonance is $\geq$ 20 Hz (same as Ref. 1).
- A minimum wall thickness is used based on manufacturing considerations.
- Side load resistance to shorting is > 13 N (3 lb_f) based on side loads possible from vapor-cooled shields).
- The orbit heat rate for six struts is approximately the same as that given in Ref. 1 for 12 PODS-I struts.
- The thin-wall tube length is kept short relative to the radius to maximize column buckling strength.

Analyses were performed to determine the optimum winding angle, α, of the thin-wall fiberglass tube. The tube wall was assumed to be made of two 0.13 mm (0.005 in.) layers, for a total thickness of 0.25 mm (0.010 in.). The inside diameter is 1.52 cm (0.600 in.) and the length is 4.17 cm (1.64 in.).

The two layers are wound at a constant angle, α, with the longitudinal axis of the tube. Thus, the angle between the filaments in the two layers is $2*\alpha$. The materials are S-glass and epoxy, for which the following data were used:

E1	Mod. of elasticity, along fibers	$5.4 \times 10^{10} N/m^2$ (7.8×10^6 psi)
E2	Mod. of elasticity, cross fibers	$0.9 \times 10^{10} N/m^2$ (1.3×10^6 psi)
G12	Shear modulus	$0.34 \times 10^{10} N/m^2$ (0.5×10^6 psi)
Nu21	Poissons ratio	0.3
Ftu1	Tensile strength, along fibers	$11 \times 10^8 N/m^2$ (160 ksi)

Ftu2	Tensile strength, cross fibers	$0.34 \times 10^8 N/m^2$ (5 ksi)
Fcu1	Compression strength, along fibers	$5.9 \times 10^8 N/m^2$ (85 ksi)
Fcu2	Compression strength, cross fibers	$1.4 \times 10^8 N/m^2$ (20 ksi)
Su12	Shear strength, along fibers	$0.62 \times 10^8 N/m^2$ (9 ksi)

The analysis was made with the aid of the STAGS C1 computer code. Some of the analysis could be made on the VAX computer, but the buckling analyses required rather large models, for which the CDC 205 computer was used. In addition to STAGS the code PANDA, which is an optimization code, was also used.

3.2.1 Tensile and Compressive Stress Levels

The stress parallel and perpendicular to the fibers for an axial strain of 0.3 percent is plotted in Fig. 9 as a function of the wind angle. The margin λ (ratio of strength value to actual stress) is plotted in Fig. 10 for compression and in Fig. 11 for tension, again at an axial strain value of 0.3 percent. (A 0.3 percent strain is the highest value the tube will see in service due to the wedge "stops" on the stem.)

At the selected wind angle of 30 deg, a margin of 8 or greater is present in all cases. (This wind angle was selected after the buckling analysis described in Section 3.3.2 was performed.)

3.2.2 Buckling Due to Axial Compression

Two different sets of analyses were made for buckling under axial compression: one with the code PANDA, and one with the code STAGS C1. The PANDA analysis is fast and inexpensive, but it is approximate in nature. The boundary conditions are simple support, rather than fixed ends (except for axial displacement of one end) as used in the STAGS analysis. Results from the PANDA analysis are given in Fig. 12, where the product λ_c* stress for buckling is plotted versus the winding angle α. The wave numbers listed are somewhat ambiguously labeled axial and circumferential; the mode, as will be seen shortly, consists of buckles arranged along a helical path, which makes

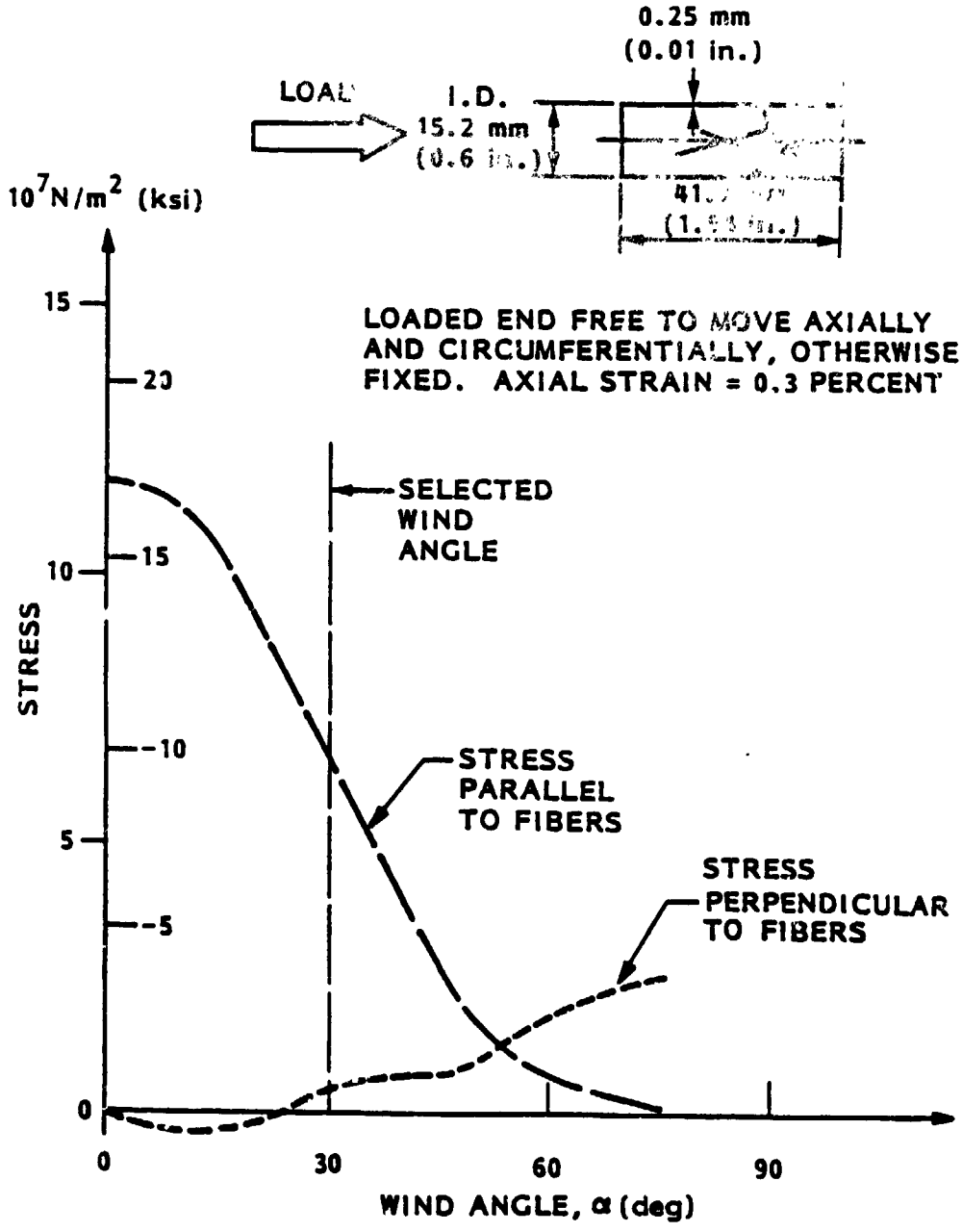

Fig. 9 Fiberglass Tube Stress Levels as a Function of the Wind Angle

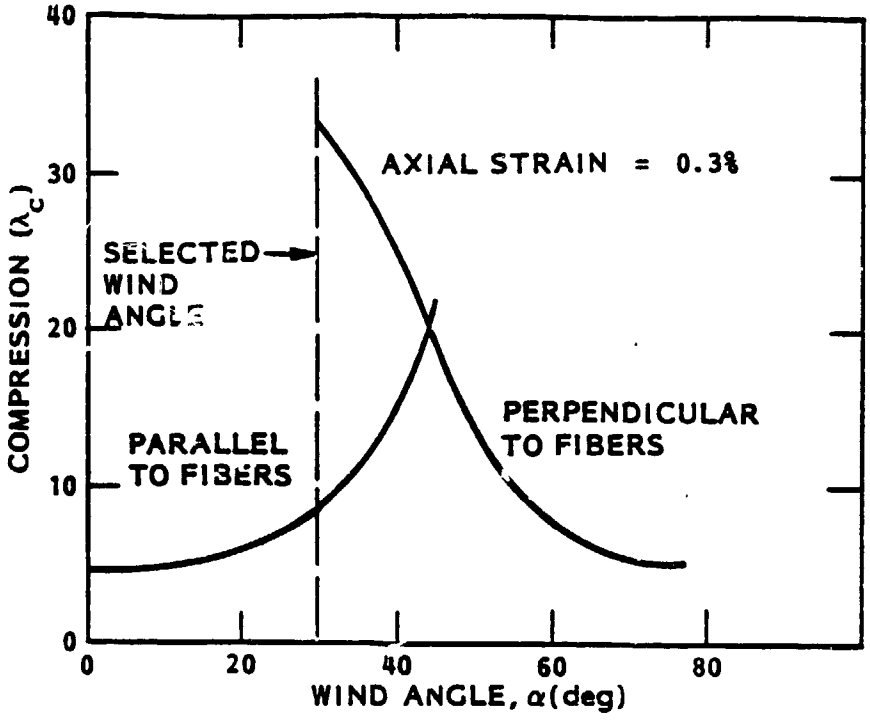

Fig. 10 Compression Stress Margin λ_c as a Function of Wind Angle

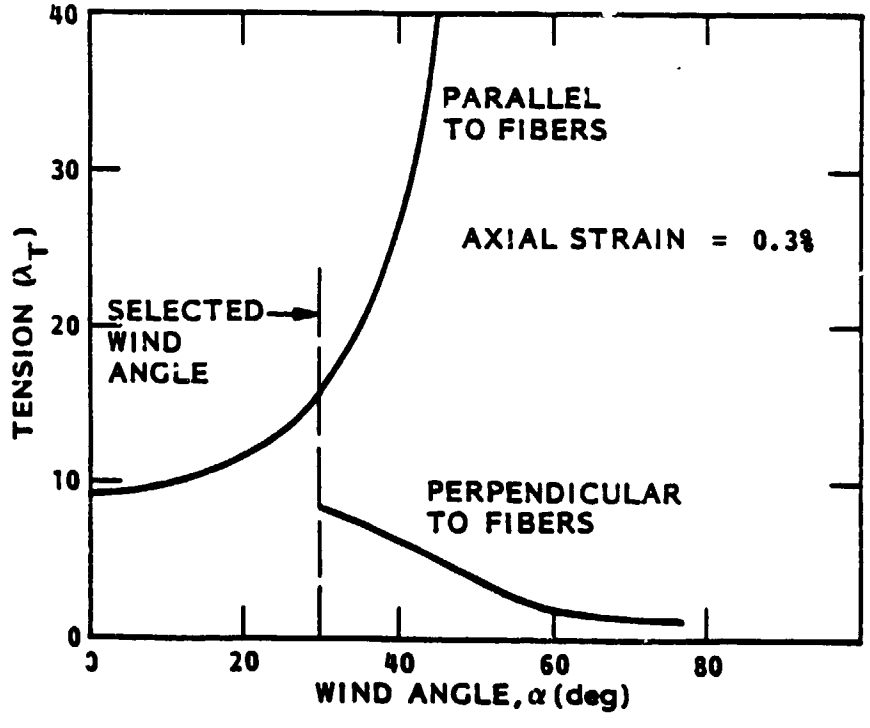

Fig. 11 Tension Stress Margin λ_t as a Function of Wind Angle

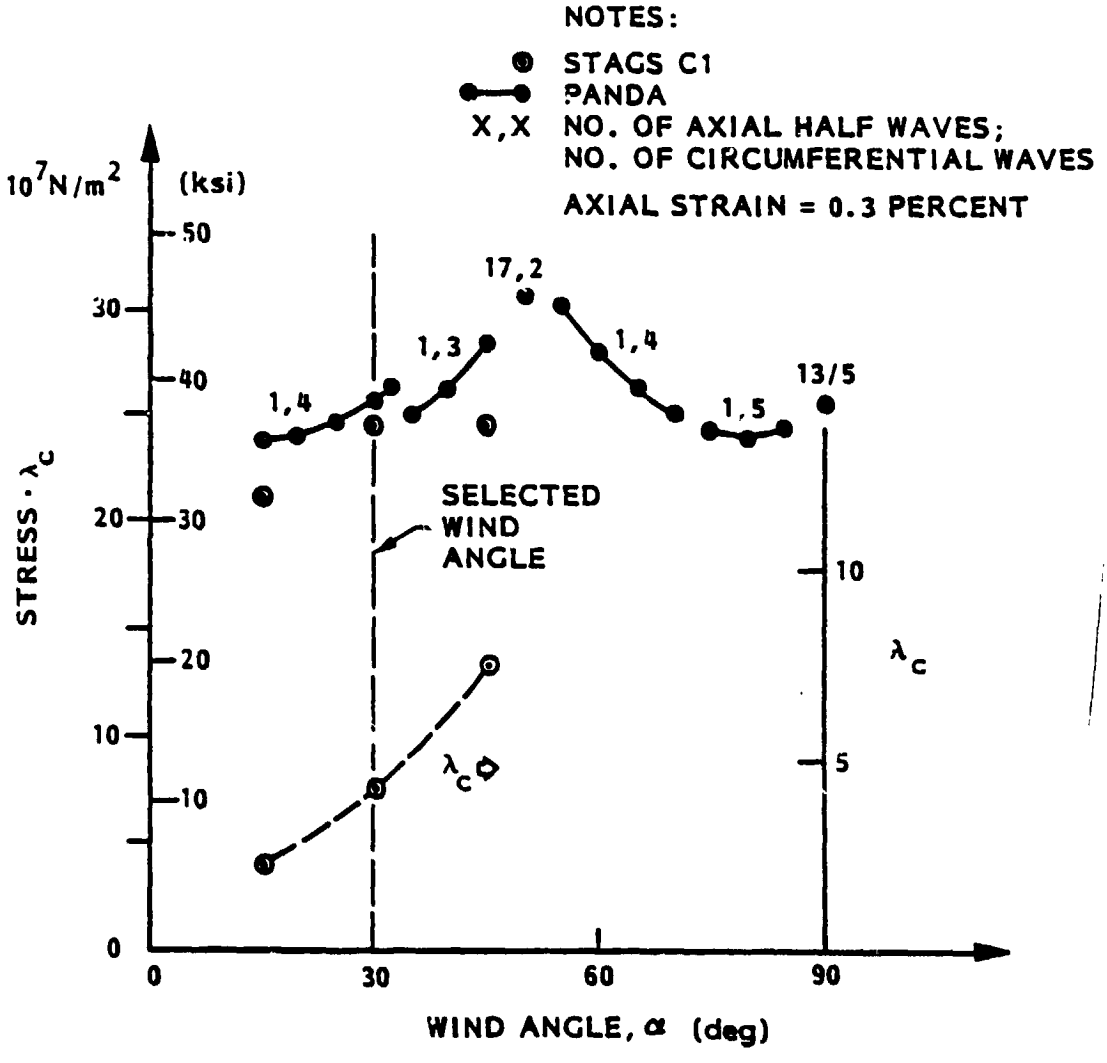

Fig. 12 Effect of Wind Angle on Buckling

the term "circumferential" mean the number of helical paths. Along each path there is one half-wave. But there are two points with a large number of axial waves (17 and 13 respectively).

In the STAGS analysis, a model with a relatively dense spacing is used. The results are also given in Fig. 12. It is interesting (and heartening) to note that the agreement with the PANDA analysis is so close. The agreement is also carried through to the mode shape, as illustrated by Fig. 13, where the mode shape for the α = 30 deg is shown. Note the helical path with three circumferential waves. (The PANDA analysis gives four waves for this case, but at α = 35 deg it gives 3 waves.)

The large number of axial waves predicted by PANDA were not seen in the STAGS analysis. There are two reasons for this: (1) the STAGS analysis was only carried out to an α value of 45 deg, which is less than the multiwave configuration predicted by PANDA; and (2) the STAGS model is too coarse (fine as it is) to accurately define the short waves. In any event, the STAGS analysis shows that a winding angle of 30 to 45 deg gives a maximum axial load capability. The prior stress analyses in Figs. 10 and 11 show more than adequate design margins exist at 30 deg, so this wind angle was selected.

3.2.3 Buckling Due to Bending

The model used for the bending analysis is similar to the one used in the axial compression analysis, but with a ring added at the loaded end to keep that end circular as it displaces laterally. The wind angle is 30 deg, and the lateral displacement of the tube at one end (with the other end fixed) is 0.18 mm (0.0072 in.). The stress variations are complex, but the maximum stress in the fiber direction is $-5.4 \times 10^7 N/m^2$ (-7800 psi), and the maximum stress across the fiber is $-7.2 \times 10^6 N/m^2$ (-1040 psi). Both stresses occur close to the fixed end. The buckling λ_b is -8.93. The minus sign is of no particular consequence; it only means that the tube buckles for a load applied in the opposite direction. But one direction is as good as the other; the second λ_b is +9.05, a number not quite converged yet. Had a few more

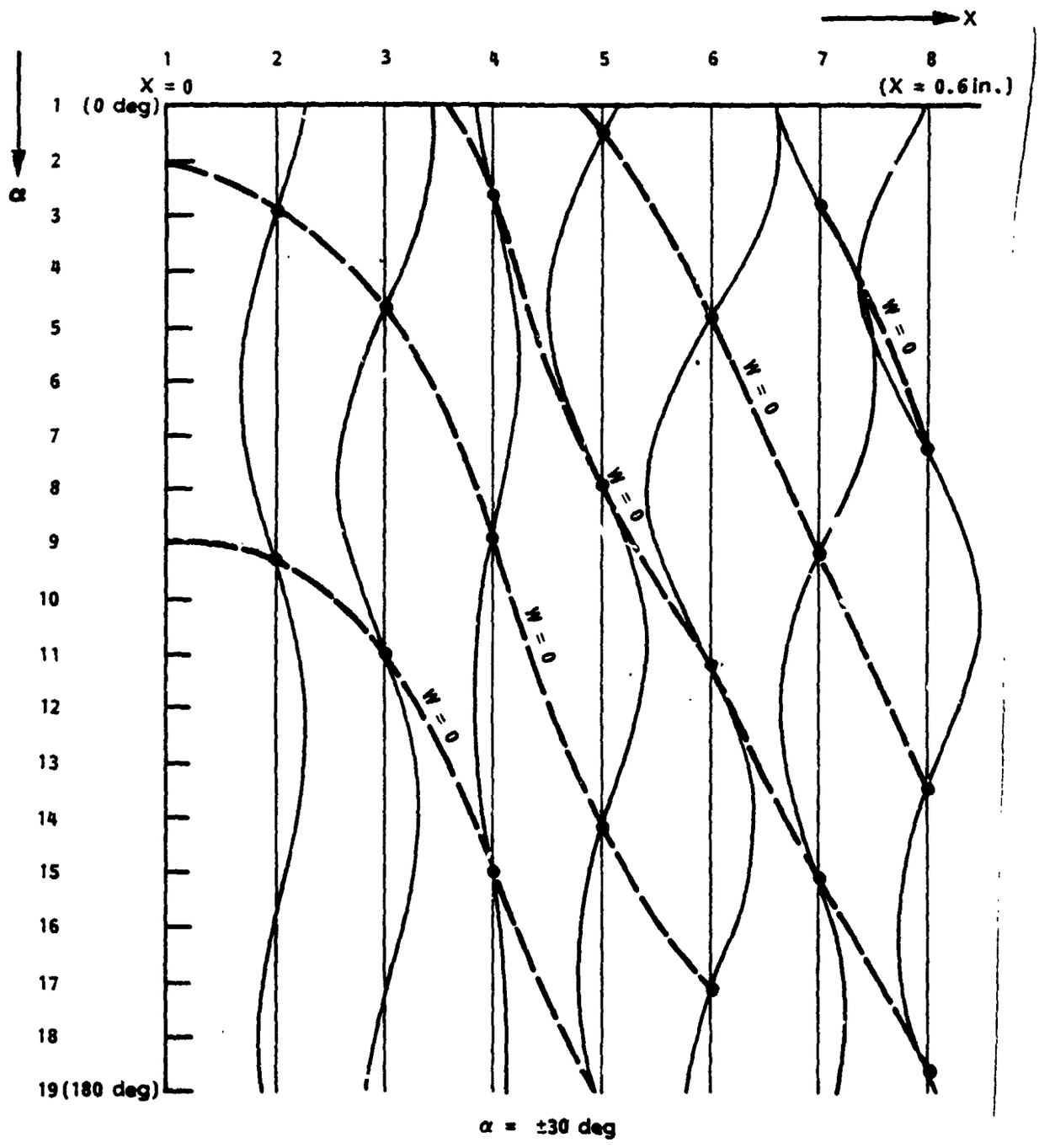

Fig. 13 Mode Shape, Axial Compression

iterations been allowed, the two numbers would have been identical. The mode shape is shown in Fig. 14. Note the lack of symmetry, which is due to the lack of symmetry in the lay-up. On one side the fibers on the outside point downwards; on the other side the fibers point upwards.

3.2.4 Side Load Deflection

To calculate the side load capability of the tube a simple beam bending formula is used.

$$y = -\frac{1}{6}\,\frac{W}{E\pi R^3 t}\,(x^3 - 3L^2x + 2L^3)$$

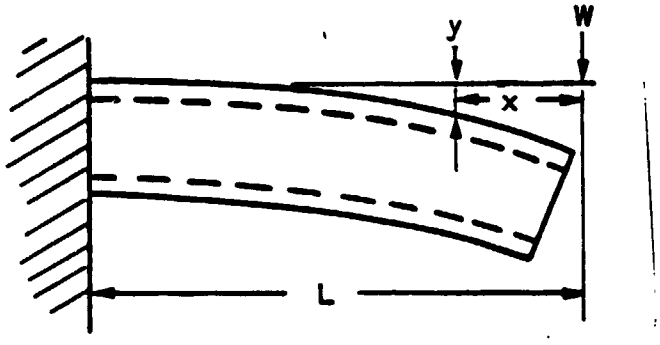

where:

- y = lateral deflection at point x
- W = side load
- R = tube outer radius
- t = tube wall thickness
- L = tube length

This formula is only an approximation since it does not include shear deformation and other more complicated deformations that are occurring. However, as seen later in Section 4, the agreement with experimental data is to within 12 percent on the average.

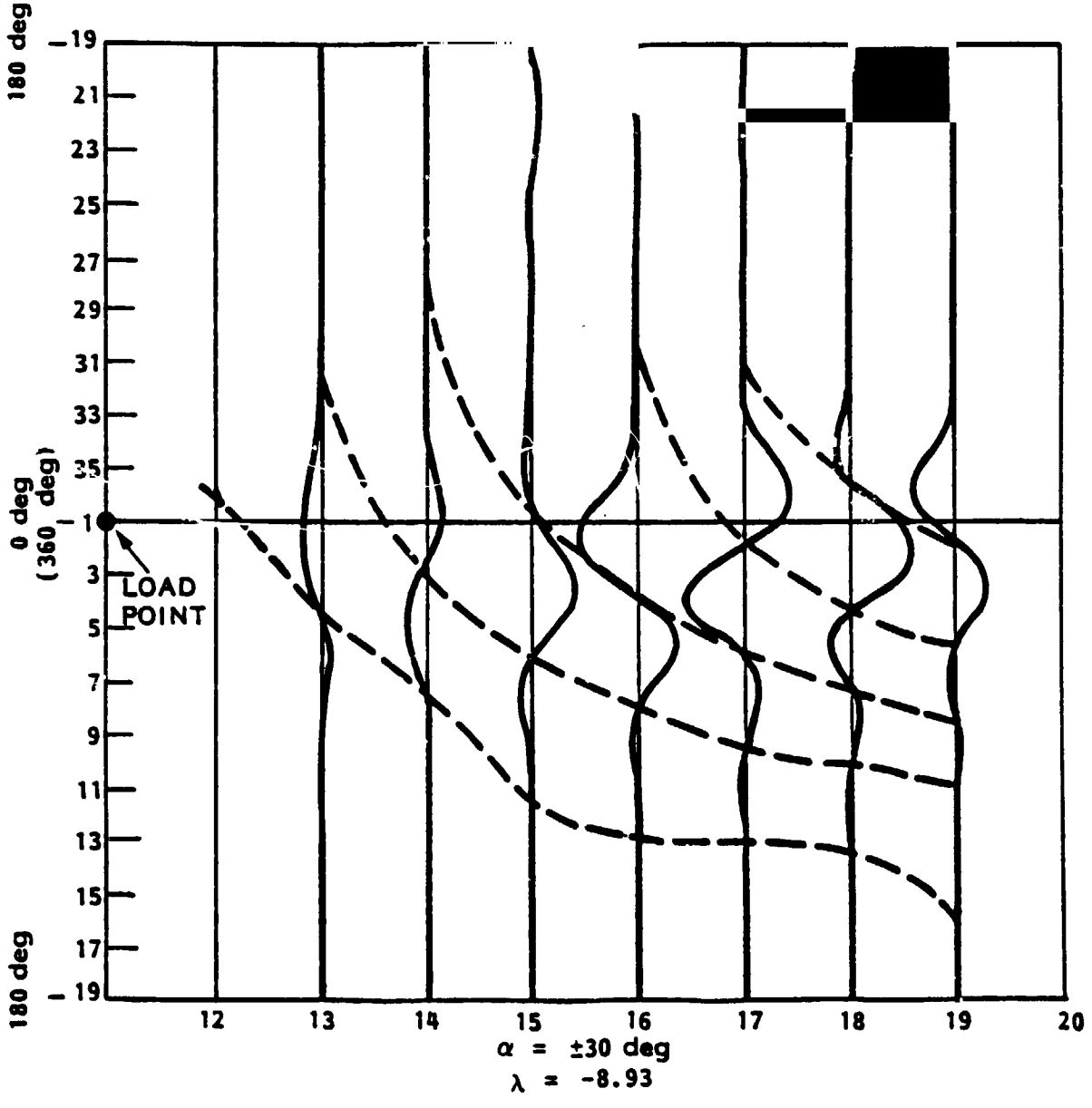

Fig. 14 Bending of Tube: Mode

3.3 THERMAL MODEL

A conduction network (Fig. 15) was programmed to predict the heat rates through the PODS-III test article. This network includes only conduction, since radiation heat transfer between the body and stem amounts to less than 2 percent of the solid conduction at 40 K, the highest boundary temperature to be tested. The contact resistances of the gold-coated threaded body/adjustment bushing and stem/thermal link were assumed to be zero. The length of resistors R_3 and R_4, 0.0417 m (1.64 in.), were divided by a cos 30 deg term to take into account the winding angle of the fiberglass filaments, effectively increasing the filament or epoxy lengths and decreasing the heat rate down the tube.

The cross sectional area of the S-glass was obtained by multiplying the tube cross sectional area by the volume fraction of glass, 0.636. The cross sectional area of epoxy was obtained by multiplying the tube cross sectional area by the volume fraction of epoxy, 0.364. Thermal conductivity values used in the analysis are provided in Table 1.

Table 1 THERMAL CONDUCTIVITY OF PODS-III MATERIALS

Temp. (K)	Thermal Conductivity (W/mK)			
	828 Epoxy (Ref. 2)	S-2 Glass* (Ref. 3)	Invar (Ref. 4)	316 Stainless Steel (Ref. 5)
2	0.034	0.036	0.10**	0.10**
4	0.046	0.110	0.23**	0.24
6	0.046	0.173	0.40**	0.39
8	0.047	0.219	0.60**	0.58
10	0.051	0.243	0.80**	0.77
15	0.070	0.296	1.3	1.30
20	0.083	0.326	1.8	1.95
25	0.093	0.357	2.2	2.6
30	0.107	0.371	2.7	3.3
35	0.115	0.382	3.2	4.0
40	0.122	0.411	3.7	4.6

*By finite difference method. S-Glass conductivity obtained from uniaxial S-Glass/Epoxy Data using volume fraction method.
**Extrapolated Data

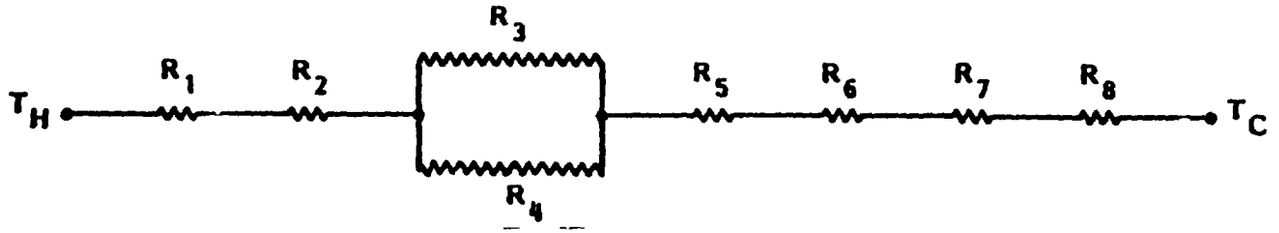

Part	Resistor	Material	Area (m^2)	Length (m)	A/L(m)
Body/Adjustment Bushing	R_1	INVAR	1×10^{-4}	0.013	0.0077
Bond Line	R_2	EPOXY	3.7×10^{-4}	0.00013	2.85
Fiberglass/Epoxy	R_3	S2-GLASS	0.1079×10^{-4}	0.0481	0.000224
Fiberglass/Epoxy	R_4	EPOXY	0.0618×10^{-4}	0.0481	0.0001285
Bond Line	R_5	EPOXY	3.7×10^{-4}	0.00013	2.85
Stem	R_6	INVAR	2.0×10^{-4}	0.0295	0.0068
Rod End (Thermal Link)	R_7	316 S.S.	0.6×10^{-4}	0.0066	0.009
Rod End (Thermal Link)	R_8	316 S.S.	0.3×10^{-4}	0.0089	0.0034

Fig. 15 PODS-III Test Article Conduction Nodal Network

Section 4
THIN-WALL FIBERGLASS TUBE STRUCTURAL TESTS

Two thin-wall fiberglass tubes were manufactured, one for a series of structural tests and one for installation into the PODS-III test article for the liquid helium thermal tests.

4.1 FIBERGLASS TUBE PROPERTIES

Dimension, weight, and volume measurements were made on thin-wall fiberglass tubes as shown in Table 2.

Table 2 PROPERTIES OF S-2 FIBERGLASS/828 EPOXY THIN WALL TUBES

	Tube for Structural Tests	Tube for PODS Thermal Tests
Density, g/cm^3	2.01*	2.01
Wall Thickness, mm(in.)	0.312 (0.0123)**	0.345 (0.0136)
Cross Sectional Area, m^2 ($in.^2$)	1.53×10^{-5} (0.0237)**	1.7×10^{-5}(0.0263)
Length, m (in.)	0.05657 (2.227)	0.05687 (2.239)
Inside Diameter, m (in.)	0.01527 (0.601)	0.01527 (0.601)
Outside Diameter, m (in.)	0.01589 (0.6256)**	0.01596 (0.6282)
Weight Percent Glass	78.8	78.8*
Volume Percent Glass	63.6	63.6*

*Based on measured value of other tube.
**Thickness adjusted based on water immersion test of other tube.

The composite density was obtained by weighing the tube first in air and then in water. The wall thickness was first calculated from direct measurements (an average of six) of the inside and outside diameter. Due to the wavy outer surface, the accuracy of this method is in question. The average wall thickness was determined for the thermal test tube more accurately by knowing the tube volume (from the water displacement weighings), inside diameter, and lengtn. The wall thickness for the t be used in the structural tests is based on the direct diameter measurements, adjusted for the water immersion tests of the thermal tube. (The thermal tube wall thickness is 0.381 mm by direct measurement and 0.345 mm by the water immersion method. It is felt that the water immersion method is more accurate since the direct measurement of the O.D. picks up the high spots but not the low spots on the tube. Consequently, it is reasonable to expect that the true average wall thickness is less than that obtained by direct measurement.) The wall thickness of the structural tube was adjusted by a factor of (0.345/0.381) = 0.91. (The water immersion test was not thought of until after the structural tube had been failed in an ultimate compression test.) The weight percent glass was determined by wet ashing the epoxy with hot H_2SO_4 and HNO_3. The glass volume percent was calculated as follows:

$$\text{Volume Percent} = \frac{(\text{Weight Percent})\ (\text{Density of Composite})}{(\text{Density of Glass})}$$

4.2 RADIAL (SIDE) LOAD DEFLECTION TEST

A radial (side) load deflection test was performed as shown in Fig. 16. Threaded aluminum end fittings were bonded into the ends of the fiberglass tube. One end of the fiberglass tube was hard mounted, and weights were hung from a rod-end fitting at the other end, located so that the rod end simulated the actual design length. Deflections were measured using a reference bar and depth gage which could be read to 0.0001 in. The measurements were taken at the middle of the fiberglass tube (point A), the end of the fiberglass tube (point B), and the location of the wedge part of the stem (point C). It was difficult to determine if the one end was truly hard mounted; the threads can slip allowing a larger deflection to be measured than actually occurs, due to tube bending only. (In the actual design, the threads will be bonded.)

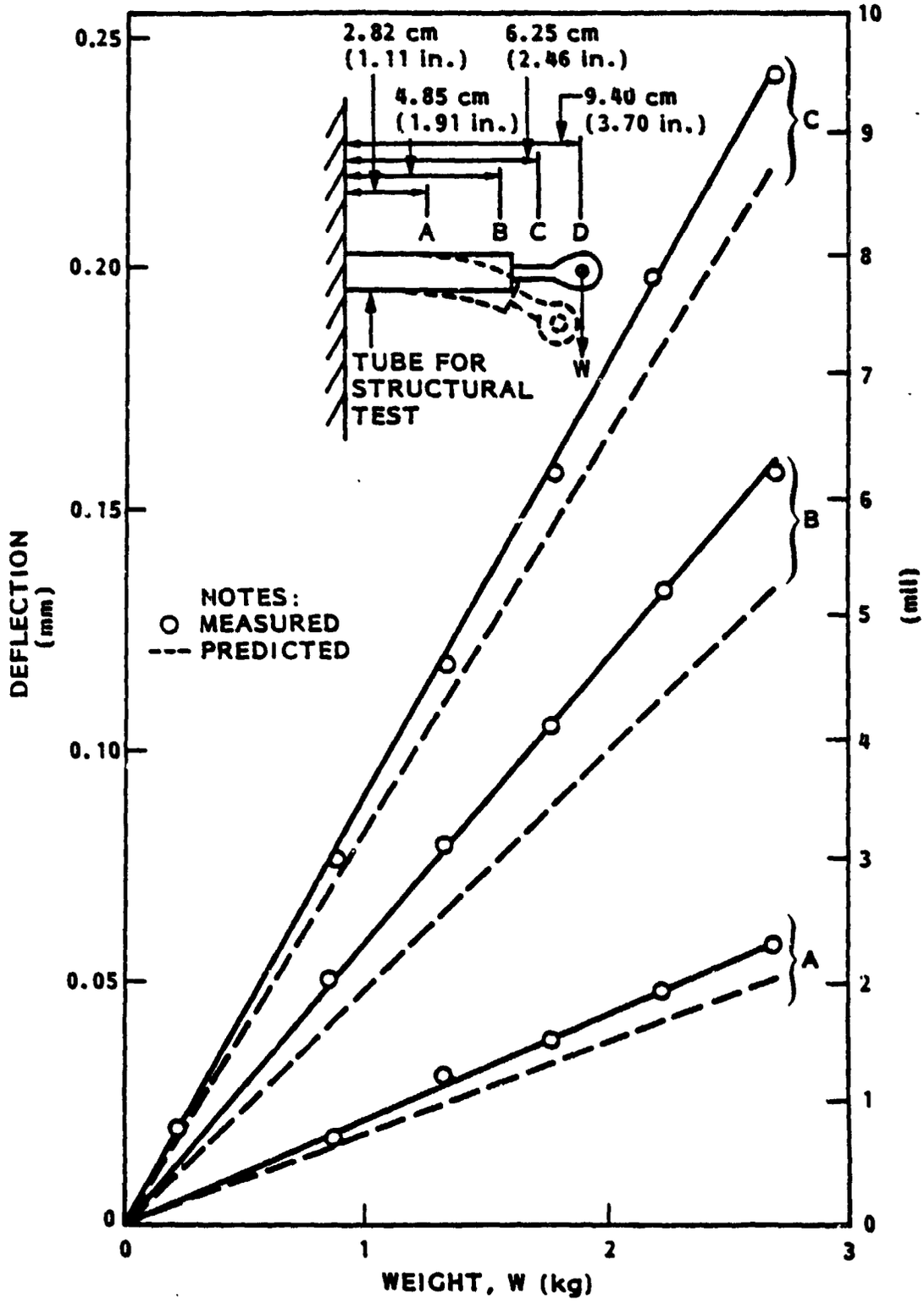

Fig. 16 Radial (Side) Load Deflection Test

However, from the straight line relationships that were measured, it appears that minimal slippage occurred. The predicted deflection is also shown on Fig. 16 using the cantilever beam formula given previously in Section 3.2. (The beam model assumes a uniform fiberglass/epoxy tube out to point D.) The predicted values are 13 percent low at point A, 16 percent low at point B, and 8 percent low at point C.

4.3 MODULUS TESTS

Precision strain gages, Model EA-13-062TV-350 from Micro-Measurements, were epoxy bonded on opposite sides of the center of the structural fiberglass tube. Threaded aluminum end fittings were epoxy bonded into each end of the tube; spherical/bearing rod end fittings, SWRMLH-4-100 from Southwest Products, were threaded into the aluminum ends, and the specimen was placed in a load machine. The distance between rod ends was 9.80 cm (3.86 in.).

Modulus tests were conducted on the structural test tube at 0.3 percent strain and at 295 (ambient air) and 78 K (immersed in liquid nitrogen).

	Modulus, N/m^2 (psi)	
	Tension	Compression
295 K	3.4×10^{10} (5.0×10^6)	3.4×10^{10} (5.0×10^6)
78 K	5.1×10^{10} (7.4×10^6)	5.2×10^{10} (7.5×10^6)
4 K (Extrapolated from Fig. 17)	5.2×10^{10} (7.5×10^6)	5.2×10^{10} (7.6×10^6)

Using temperature-dependent modulus data from the literature on similar glass/epoxy systems allows the modulus to be extrapolated to liquid helium temperature as shown in Fig. 17.

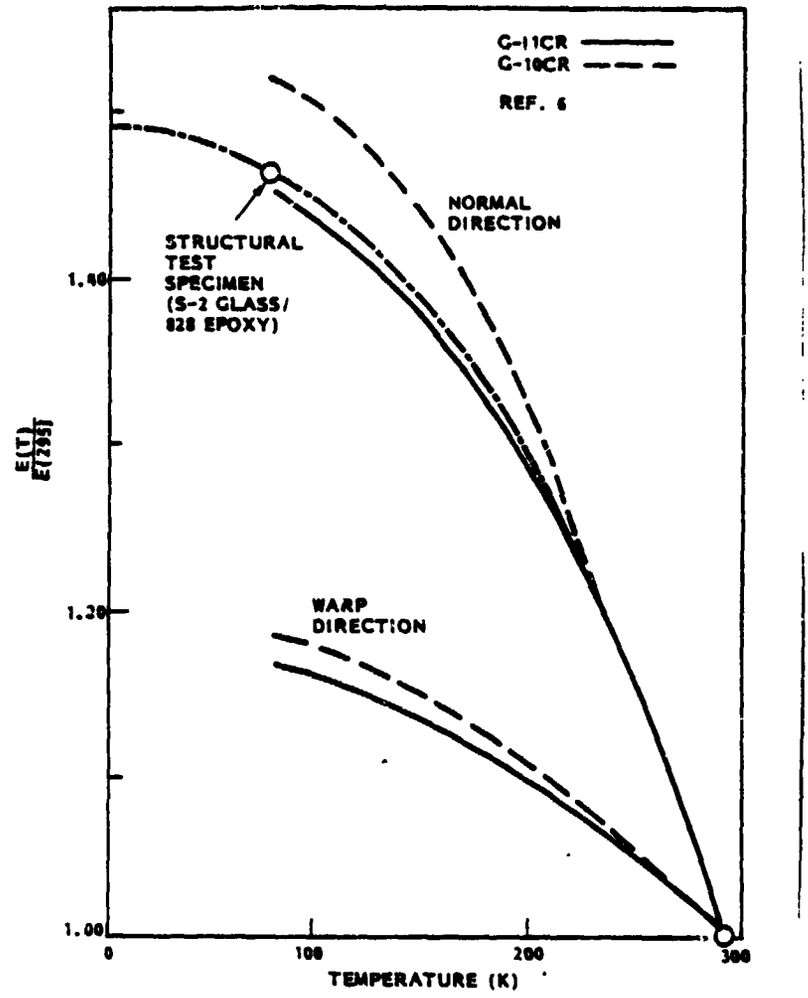

Fig. 17 Normalized Temperature Dependent Modulus Values for Fiberglass/Epoxy

4.4 ULTIMATE COMPRESSION LOAD TEST

Using the same setup used for the modulus tests, the structural fiberglass tube was failed in compression while immersed in liquid nitrogen at 78 K. The failure load of 4,890 N (1,100 lb_f) compares to a predicted value of 5,650 N (1,270 lb_f). Visual examination of the failed tube indicates that the

Fig. 18 Thin-Wall Fiberglass Tubes

failure mode may be by delamination (as shown in Fig. 18) rather than the spiral buckling mode predicted. To prevent this delamination failure mode on future tubes, the +30-deg, -30-deg weave should be interwoven at more frequent intervals than the 2- to 4-cm spacing used on this tube, and a 12 end roving should be used in place of the 20 end roving. This would also help to make a smoother outer surface on the tube.

4.5 LOAD TESTS ON THE ASSEMBLED TEST ARTICLE

4.5.1 Side Load Tests

The gap between the stem/body was set using three 0.076-mm (0.003-in.) shims. The adjustment bushing/body threads were epoxied and allowed to cure overnight. The three shims were pulled out. The nut threads were epoxied onto the body threads setting the nut/stem gap with three 0.076-mm (0.003-in.) shims. The epoxy was allowed to cure overnight, and the three shims were

pulled. (It is believed that this procedure allowed the nut to be misaligned with the stem, since the stem was unsupported. In the future, all six shims should be inserted at the same time, plus epoxy bonding of the stem/body and nut/body should be done concurrently.)

Accounting for the 30-deg angle of the stem wedge, the axial gap is 0.088 mm (0.0035 in.), and the effective radial gap accounting for the offset is 0.13 mm (0.0052 in.). Based on the modulus data shown previously in Section 4.3, the radial load deflection data shown in Section 4.2, and the gap spacing, predictions were made on values that should be obtained on an assembled test article and compared to test data as shown in Table 3.

Note that measurements were made at 60-deg increments around the circumference. In quadrants 5 and 6, the measured values were considerably lower than in quadrants 1 through 4, indicating that the fiberglass tube is not centered properly. A second test verified that the measured values are repeatable and the tube is deflecting elastically as desired.

A comparison of the average measured values with predicted values in Table 3 shows that the measured values are low by 23 percent. Using the six-shim assembly procedure, this difference should be lower on future PODS-III assemblies.

4.5.2 Axial Load Tests

The PODS-III test article was mounted in a load machine using rod-end fittings at each end as shown in Fig. 19. An ohmmeter was connected to the body and stem to monitor the shorting under load. A deflectometer measured the differential axial movement between the body and the stem. Load tests were performed in compression four times and in tension four times. This cycle was then repeated another four times. The test data are provided in Table 4. Note that the tension shorting loads are slightly higher than the compression loads, and the repeatability of the test data is good, indicating that the fiberglass tube is acting in an elastic mode as desired.

Table 3 RADIAL (SIDE) LOAD DEFLECTION TEST DATA ON PODS-III

	290 K			
	First Test		Repeat Test	
Quadrant	kg	(lb)	kg	(lb)
1	1.38	3.05	1.41	3.10
2	1.16	2.55	1.13	2.50
3	1.39	3.07	1.40	3.08
4	1.36	3.00	1.37	3.02
5	0.88	1.95	0.93	2.06
6	0.54	1.20	0.57	1.25
	1.12 ± 0.34	2.47 ± 0.76	1.14 ± 0.34	2.50 ± 0.74

	Measured W		Predicted** W	
	kg	lb	kg	lb
290 K	1.13	2.49	1.47	3.24
4 K*	1.70	3.74	2.21	4.96

*Based on increased E at 4 K.
**Based on deflection test data, Fig. 16 Curve C.

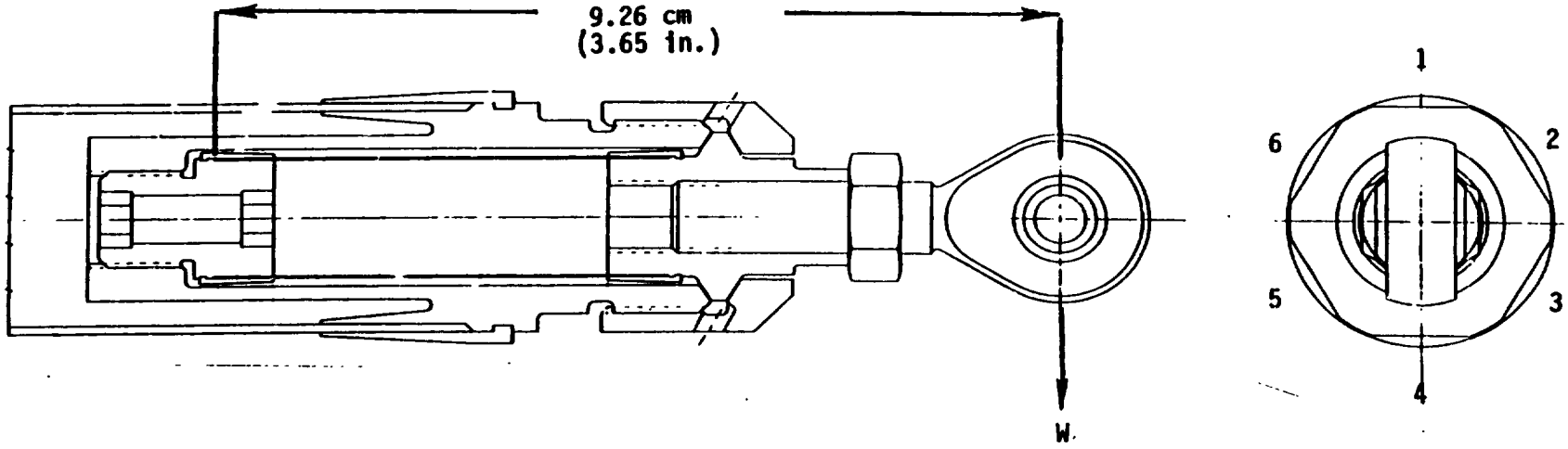

Table 4 AXIAL LOAD TEST DATA ON PODS-III

Test Seq.	Type	Shorting/ Unshorting Load			
		Load (N)	Unload (N)	Load (lb_f)	Unload (lb_f)
1	Comp	547	516	123	116
2	Comp	534	512	120	115
3	Comp	538	480	121	108
4	Comp	516	512	116	115
5	Tens.	627	583	141	131
6	Tens.	618	600	139	135
7	Tens.	618	605	139	136
8	Tens.	614	605	138	136
9	Comp	560	485	126	109
10	Comp	538	498	121	112
11	Comp	547	525	123	118
12	Comp	547	529	123	119
13	Tens.	627	609	141	137
14	Tens.	605	596	136	134
15	Tens.	609	609	137	137
16	Tens.	605	609	136	137

AVERAGE VALUES

	Compression		Tension	
	Load N (lb_f)	Unload N (lb_f)	Load N (lb_f)	Unload N (lb_f)
1st cycle, 4 ea.	534 ± 13 (120 ± 2.9)	505 ± 16.5 (113.5 ± 3.7)	619 ± 6 (139.2 ± 1.3)	598 ± 11 (134.5 ± 2.4)
2nd cycle, 4 ea.	548 ± 9 (123.2 ± 2.1)	509 ± 21 (114.5 ± 4.8)	612 ± 11 (137.5 ± 2.4)	606 ± 7 (136.2 ± 1.5)
Average, 8 ea.	541 ± 13 (121.6 ± 2.9)	507 ± 18 (114.0 ± 4.0)	616 ± 9 (138.4 ± 2.0)	602 ± 9 (135.4 ± 2.1)
Average, 16 ea.	524 (117.8)		609 (136.9)	

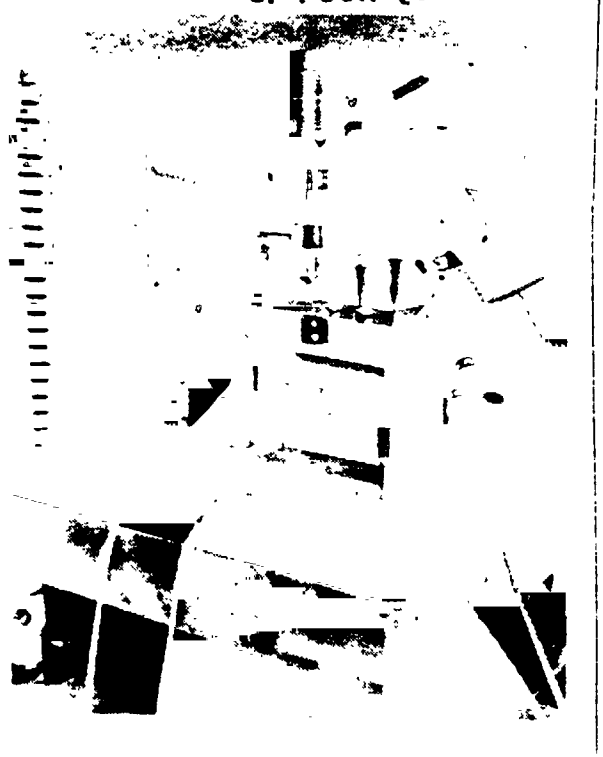

Fig. 19 Axial Load Test Setup

Based on the abrupt change in slope of the stress-strain plot obtained during these tests, the stem wedge bottoms at 970 N (218 lb_f) in compression and at 818 N (184 lb_f) in tension. The average measured "shorting" load in compression is 524 N (117.8 lb_f) or 46 percent low. The average measured shorting load in tension is 609 N (136.9 lb_f) or 26 percent low. The large discrepancy is probably due to the misalignment problem discussed previously in Section 4.5.1. Using the recommended 6-shim assembly procedure, the "shorting" load should more closely approach the load when the wedge stem bottoms. The 6-shim assembly procedure will be demonstrated during the structural development tasks this year.

4.6 THERMAL EXPANSION TESTS

Thermal expansion measurements were made over the range 394 to 116 K for the bonded Invar adjustment bushing/small fiberglass tube/Invar stem assembly and

a 1.59-cm (0.625-in.) diameter Invar rod 7.62 cm (3.00 in.) long. The Invar ΔL values for the adjustment bushing and stem length were subtracted from the ΔL values for the assembly to obtain the fiberglass tube ΔL values. The $\Delta L/L$ values for the Invar rod and the fiberglass tube are given in Table 5 and plotted in Fig. 20. The $\Delta L/L$ values are extrapolated from 116 K down to 2 K based on literature data for similar materials.

Using the $\Delta L/L$ data at 8.6 K for the fiberglass tube (HE0014) and at 15 K for the Invar body, the fiberglass tube contracts more than the body by:

$$\left[L\left(\frac{\Delta L}{L}_{F.G.}\right)-\left(\frac{\Delta L}{L}_{INVAR}\right)\right] \text{ or}$$

$$4.145\ (0.00145 - 0.00048) = 0.0040 \text{ cm } (0.0016 \text{ in.})$$

The temperatures selected were based on the first vapor-cooled shield temperature taken from Ref. 1 (with the vacuum shell at 200 K).

Table 5 THERMAL EXPANSION DATA (PERCENT)

Temperature (K)	Invar	Fiberglass Tube HE0014
116.5	-0.0310	-0.0997
130.4	-0.0275	-0.0933
144.3	-0.0240	-0.0864
158.2	-0.0207	-0.0802
172.1	-0.0179	-0.0736
185.9	-0.0151	-0.0663
199.8	-0.0127	-0.0583
213.7	-0.0105	-0.0494
227.6	-0.0083	-0.0406
241.5	-0.0062	-0.0343
255.4	-0.0043	-0.0257
269.3	-0.0027	-0.0164
283.4	-0.0011	-0.0070
292.6	0	0
297.1	0.0006	0.0033
310.9	0.0018	0.0137
324.8	0.0031	0.0242
338.7	0.0045	0.0339
352.6	0.0062	0.0415
366.5	0.0080	0.0414
380.4	0.0106	0.0321
394.3	0.0130	0.0040

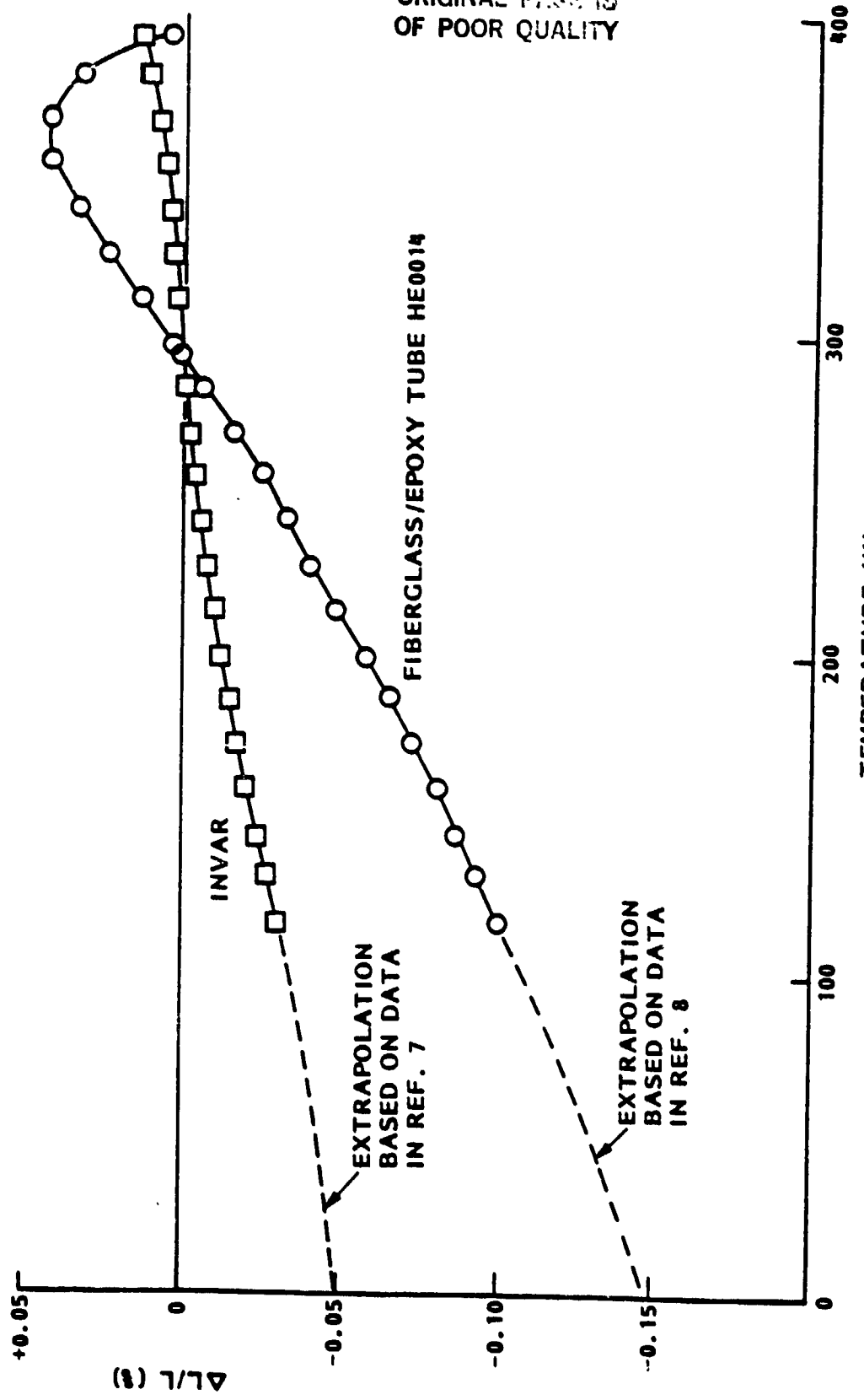

Fig. 20 Thermal Expansion Data

Section 5
PODS-III ASSEMBLY PROCEDURES

5.1 INTRODUCTION

The parts making up the PODS-III test article are shown in Fig. 21. The assembled adjustment bushing/thin-wall fiberglass tube/stem is shown in Fig. 22. The completely assembled test article is shown in Fig. 23. The parts and steps required to assemble the test article based on the test results are provided in this section.

5.2 REQUIRED PARTS AND ASSEMBLY MATERIALS

- Stem HE 009* (Fig. 3)
- Nut HE 0010* (Fig. 4)
- Body HE 0011* (Fig. 5)
- Adjustment Bushing HE 0012* (Fig.6)
- Clamshell HE 0013* (Fig. 7)
- Fiberglass/Epoxy Tube HE 0014 (Fig. 8)
- Assembly Tool HE 0015 (Fig. 24)
- Epoxy Adhesive Epibond 1210-A
  100 parts by wt
  Hardener 9615-10
  50 parts by wt
  (Lockheed Part No. 30-551-0850500)
- 1/2-in. Heat Shrink Teflon Tubing
- White Lint Free Dacron Gloves
- Holding Block (Fig. 25)
- 0.0048 and 0.002-in. shims, 3 ea, 0.050 x 2 in.
- 4 mil glass beads
- Safety wire, 20 mil
- Kapton Tape, LAC24-4450C
- Distilled water
- MEK
- 320 Grit Emery Paper
- Trichloroethane

*Parts to be nickel and gold coated and vacuum baked out per callouts on the drawing.

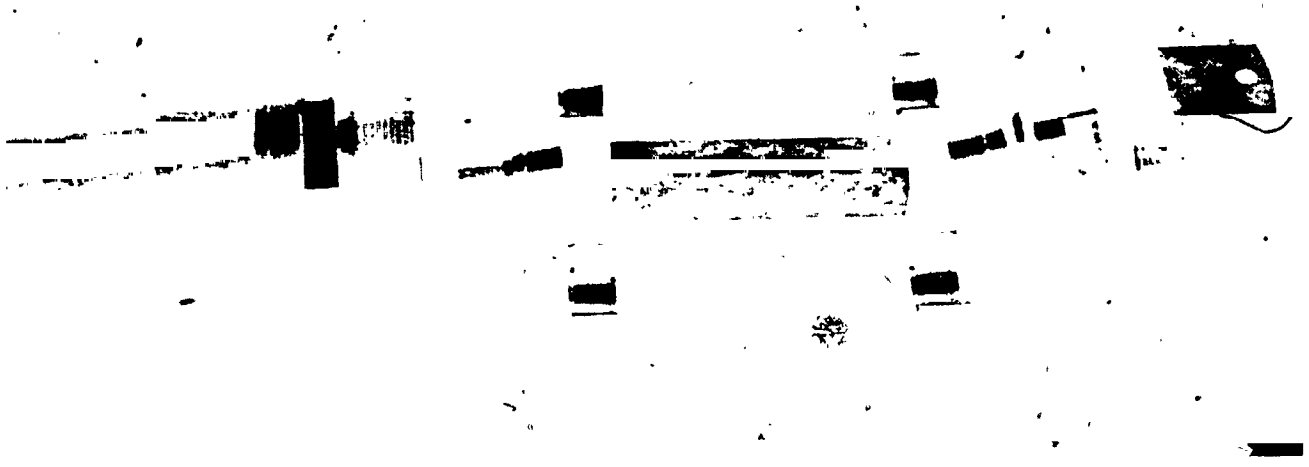

Fig. 21 PODS-III Parts (Test Article)

Fig. 22 Adjustment Bushing/Thin-Wall Fiberglass Tube/Stem Subassembly

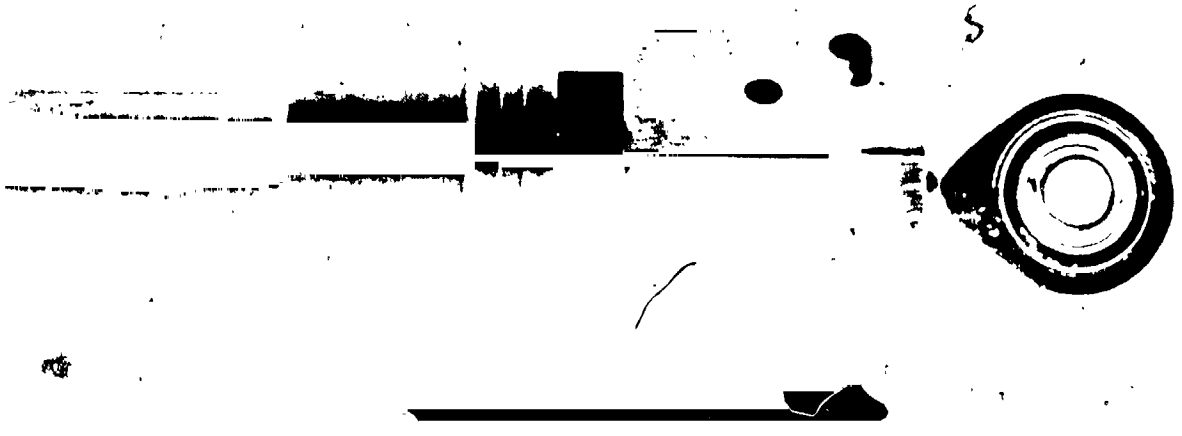

Fig. 23 PODS-III Assembly (With Rod End)

NOTES:
1. SURFACE FINISH $\sqrt{32}$ MAX.
2. MACHINE PER SPEC LAC 3601.
3. CLEAN PER SPEC LAC 0170.
4. PROTECT PER SPEC LAC 1001.
5. IDENTIFY PER SPEC LAC 3575-011998.

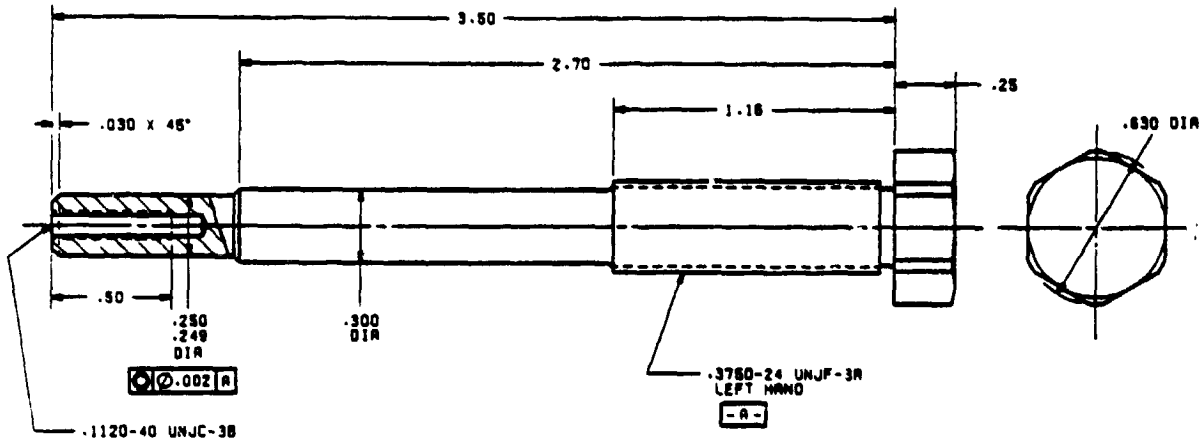

Fig. 24 Assembly Tool

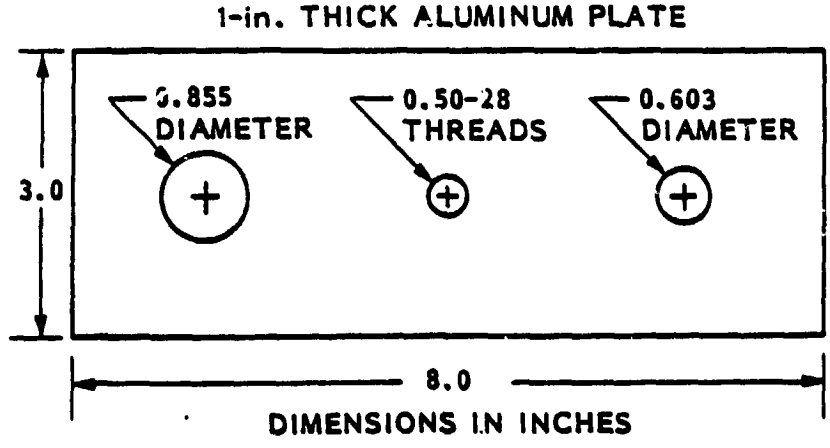

Fig. 25 Holding Block

5.3 ASSEMBLY STEPS

1. Dimensionally check all parts prior to assembly. Record dimensions of the fiberglass tube.
2. Wet ash a separate fiberglass tube from the same lot to determine the weight percent of glass and epoxy.
3. Handle all parts with clean, white, lint free gloves. Rinse the following parts with MEK (HE 0009, -10, -11, -12, -13). Rinse the assembly tool; heat shrink Teflon tubing and glass beads with MEK. Use only oil free, clean tools for assembly.
4. Hand sand the inside and outside surface of both ends of the fiberglass tube (0.4 in. axially) with 320 grit emery paper to remove the surface gloss. Sand so that the marks form circumferentially around the part. Measure the average wall thickness of the tube using the water immersion method described in Section 4.1.
5. Place the fiberglass tube into trichlorethane (immersed in an ultrasonic bath) for one minute. Remove and rinse the tube with distilled water and air dry. No water break shall occur upon rinsing within one minute after withdrawal from the water in the sanded areas.
6. Cover the groove area on the stem (Fig. 3) and the adjustment bushing (Fig. 6) with heat-shrink Teflon tubing. Apply a hot air gun to shrink the tubing.

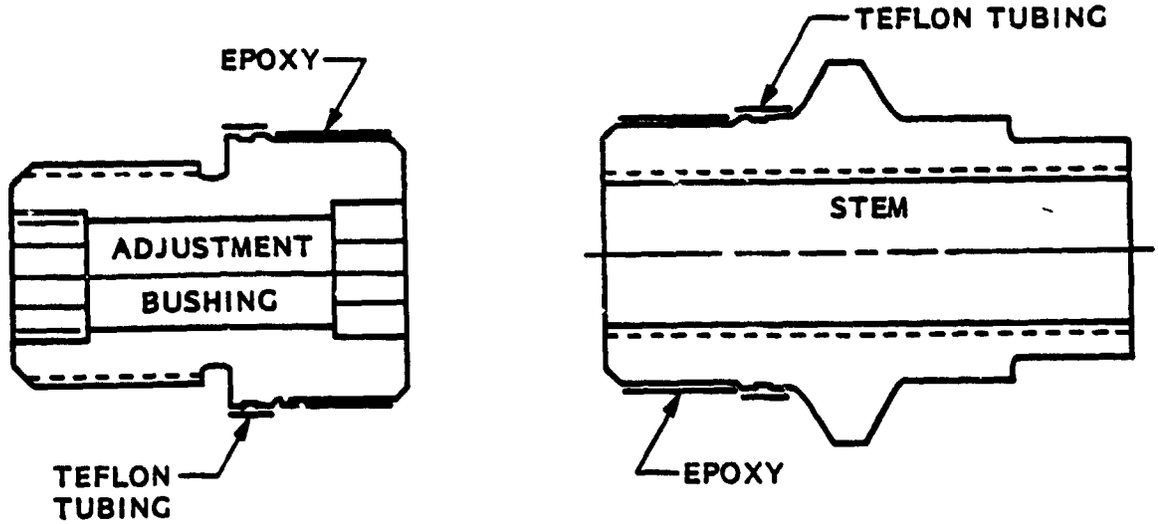

7. Steps 7 and 8 must be done within one hour. Cover with a thin layer of epoxy (with 5 percent by weight glass beads added) the O.D. of the stem (Fig. 3) where shown and the I.D. of both ends of the fiberglass tube (Fig. 8) to an area 0.3 in. from the end. Push the tube into the stem, checking visually to make certain no voids exist in the bond line. Cover the O.D. of the adjustment bushing (Fig. 6) with epoxy (with 5 percent by weight glass beads added) where shown, and push onto the other end of the tube. Screw the assembly tool into the stem (Fig. 26A). Check both bondlines for bubbles or gaps. Place a screw/washer/rubber hex in the other end to hold the assembly together. Remove all excess epoxy with a spatula.
8. Clamp the holding block (Fig. 25) in a vise so that the body (Fig. 5) can be inserted through the hole in a vertical position with the smaller female threaded end pointing down. Lower the bonded assembly (stem, tube, adjustment bushing) into the body. Screw the adjustment bushing part way into the body using the hex on the assembly tool. Keep screwing in the bushing until the stem seats in the body. Check around the circumference to make sure that the cone shaped surfaces of the stem and body are firmly seated. Screw on the nut (Fig. 4) until it seats firmly against the stem wedge (Fig. 3). The time elapsed from first mixing the epoxy until this point in the assembly should be <u>less</u> than one hour. Allow the epoxy to cure overnight.
9. Remove the nut (Fig. 4), unscrew the adjustment bushing (Fig. 6), and remove the bonded part (Fig. 26B). Cut the Teflon sleeve off the adjustment bushing (Fig. 6). Cut back the Teflon sleeve on the stem (Fig. 3) so that the groove is exposed. Using 320 grit paper, sand the ends of the tube over a 0.3-in. length (to remove the gloss from any new epoxy). Clean the tube (Fig. 8) with a trichloroethane rinse and air dry. Screw the adjustment bushing (Fig. 6) into the threaded hole in the holding block. Degrease the clamshell parts (Fig. 7) in MEK and air dry. Coat the inside surfaces of the clamshell parts (Fig. 7) and the mating fiberglass tube/groove area on the bonded bushing/fiberglass tube/stem assembly with a thin layer of epoxy. (Add 5 percent by weight of glass beads.) Place each clamshell

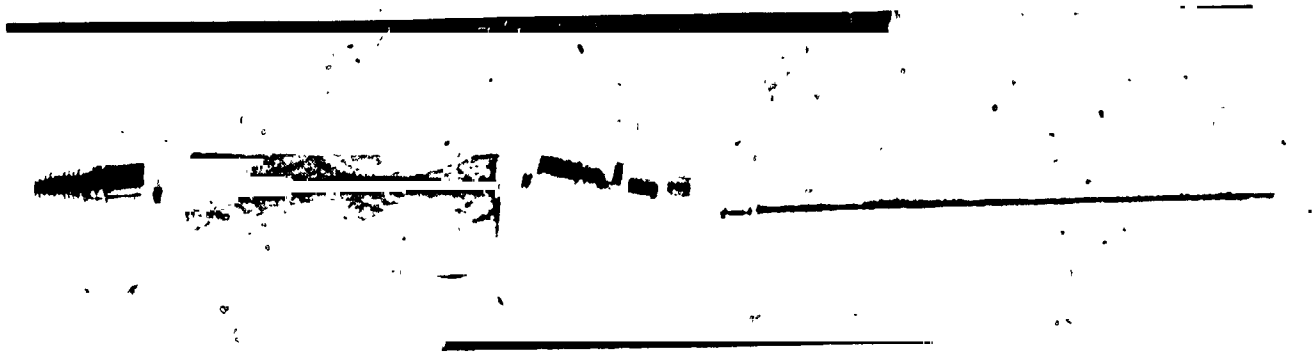

A. Parts Plus Assembly Tool

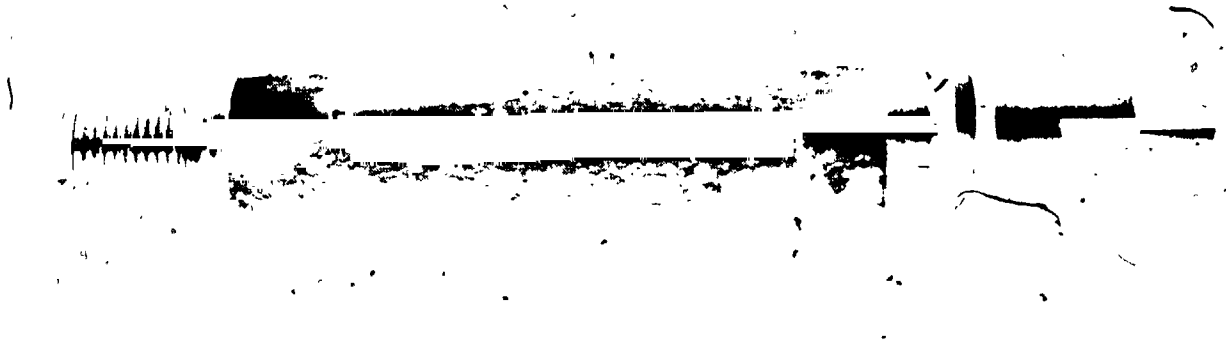

B. Initial Bonding Step

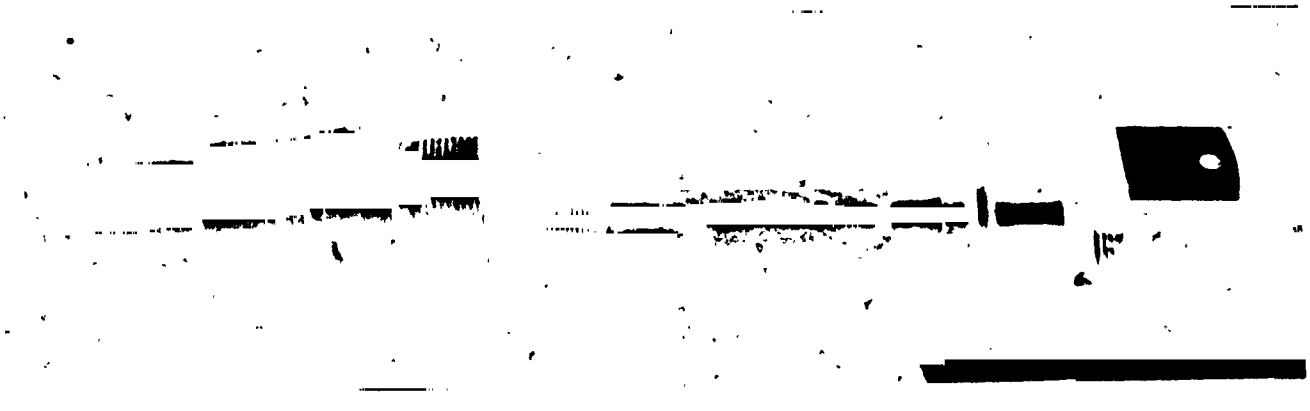

C. Final Bonding Step

Fig. 26 Fiberglass Tube Assembly Steps

(Fig. 7) on top of a 1-in.-high block and guide the clamshell lip into the adjustment bushing (Fig. 6) or stem (Fig. 3) groove. Assemble the clamshell halves (Fig. 7) on each end so that the joint is rotated 90 deg with respect to each other. Hold the clamshells (Fig. 7) in place with safety wire wrapped twice and then twisted. Remove excess epoxy with a metal spatula followed by a Q-tip. Allow to cure overnight. Remove the safety wire and Teflon sleeving. Clean off excess epoxy with a scalpel. Remove the assembly tool.

10. Place a thin layer of epoxy on the mating body threads and screw the adjustment bushing (Fig. 6) into the body (Fig. 5) until the stem (Fig. 3) seats. Back off 1/8 of a turn. Place a thin layer of epoxy on the mating body threads and screw the nut (Fig. 4) onto the body until it seats against the stem (Fig. 3). Back off the nut (Fig. 4) 1/8 of a turn. (Parts shown in Fig. 26C.) Place the body in the holding block so that the nut (Fig. 4) is on top. Place three 4.3-mil shims through the three holes in the side of the nut (Fig. 4) between the body (Fig. 5) and stem (Fig. 3). (The shims slant upward.) Tighten the adjustment bushing (Fig. 6) until the shims are snug. Place three 2.0-mil shims through the three holes in the side of the nut (Fig. 4) between the stem (Fig. 3) and the nut (Fig. 4). (The shims slant downward.) Tighten the nut until the shims are snug. Allow the epoxy to cure overnight. Remove all 6 shims. Using an ohmmeter, check to make certain the stem (Fig. 3) and body (Fig. 5) are not shorted.

11. Perform both a side load test per Section 4.5.1 and axial compression and tension load tests per Section 4.5.2. The minimum allowable values shall be greater than:

	N	lb_f
Side Load Test		
Any of six quandrants	TBD*	TBD
Axial Load Test		
Tension	TBD	TBD
Compression	TBD	TBD

* Values will be set following more extensive testing that will be done in a follow-on program.

12. This completes the assembly procedure.

Section 6
THERMAL TESTS

Thermal tests were performed on the PODS-III test article using a calibrated thermal link to measure the heat flow from the test article to a liquid helium heat sink. Details of the instrumentation and test setup, test procedure, and test results, plus a discussion of the test results are provided in this section.

6.1 INSTRUMENTATION AND TEST SETUP

Parts of the overall test setup are shown in Fig. 27. A cross section of the PODS-III test article, thermal link, and bottom part of the helium tank is shown in Fig. 28.

Note that the thermal link is conductively coupled to the helium heat sink through a 0.95-cm (3/8 in.) thick copper plate using brass screws and an indium gasket. The threaded end of the stainless steel thermal link simulates the rod-end fitting on which the PODS-III test article is mounted. Four layers of double aluminized Mylar and Dacron net are spiral wrapped onto a Mylar cage around the test article as shown in Fig. 28 without touching the test article or the 4.3-K copper tank surrounding it.

The electrical schematic for the four temperature sensors, two heaters, and "short" detector are shown in Fig. 29. Characteristics of the four-wire temperature sensors and heaters are provided in Table 6. A constant current source for the temperature sensors varies less than 0.01 percent over the range of ambient temperature experienced in the laboratory. As a check on the current, voltage is measured across a standard resistor in one leg of all temperature sensors as well as the two heaters.

Thermal Link Assembly

PODS-III Article
Installed on Thermal
Link

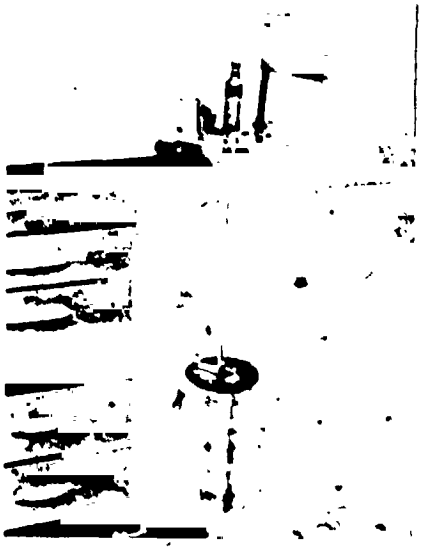

LHe Test Tank

LN_2 Guarded Helium Dewar with
High Vacuum Pumping Station and
Data Acquisition System

Fig. 27 Test Setup

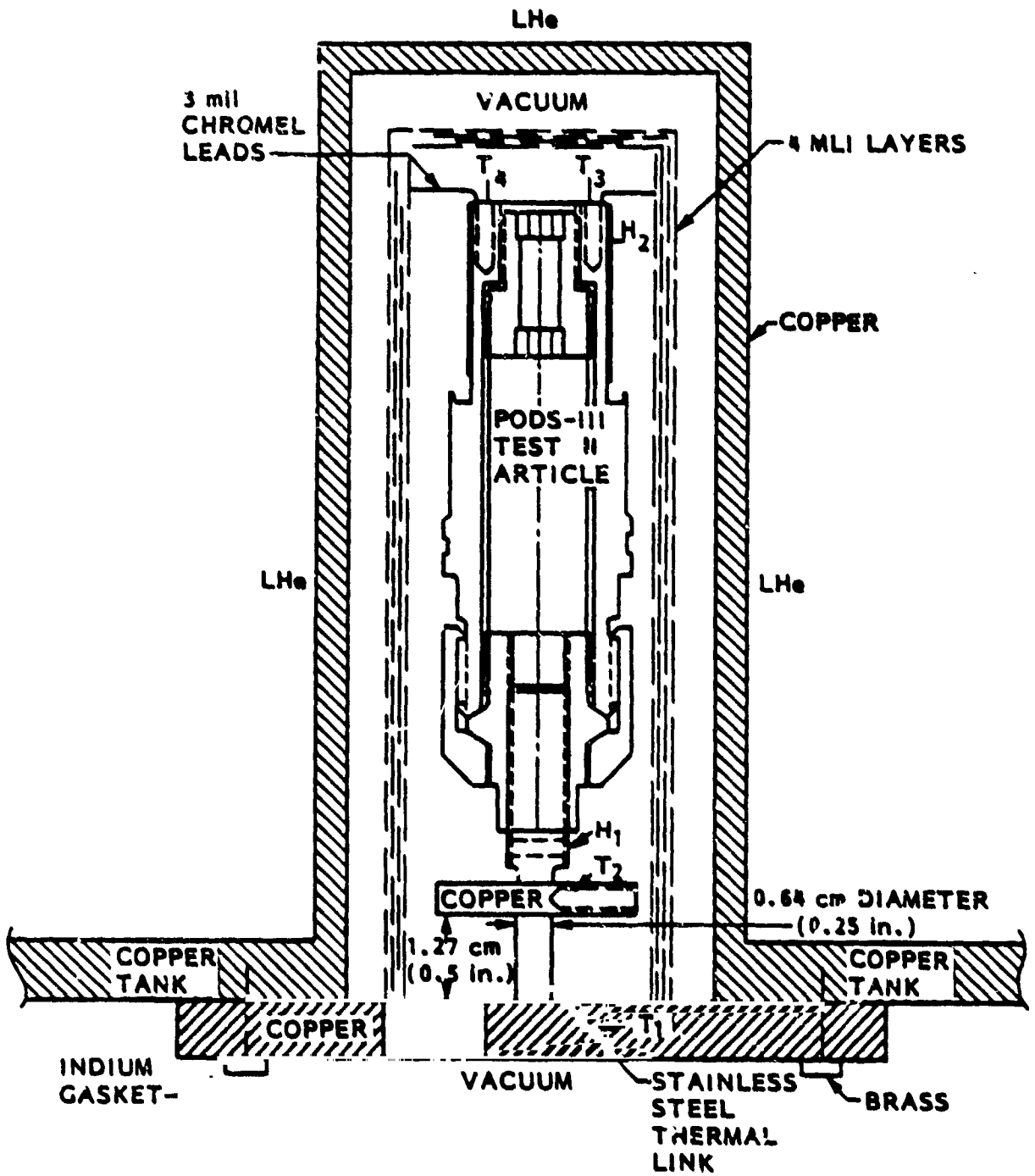

Fig. 28 PODS-III Test Article Installed in the Helium Test Tank

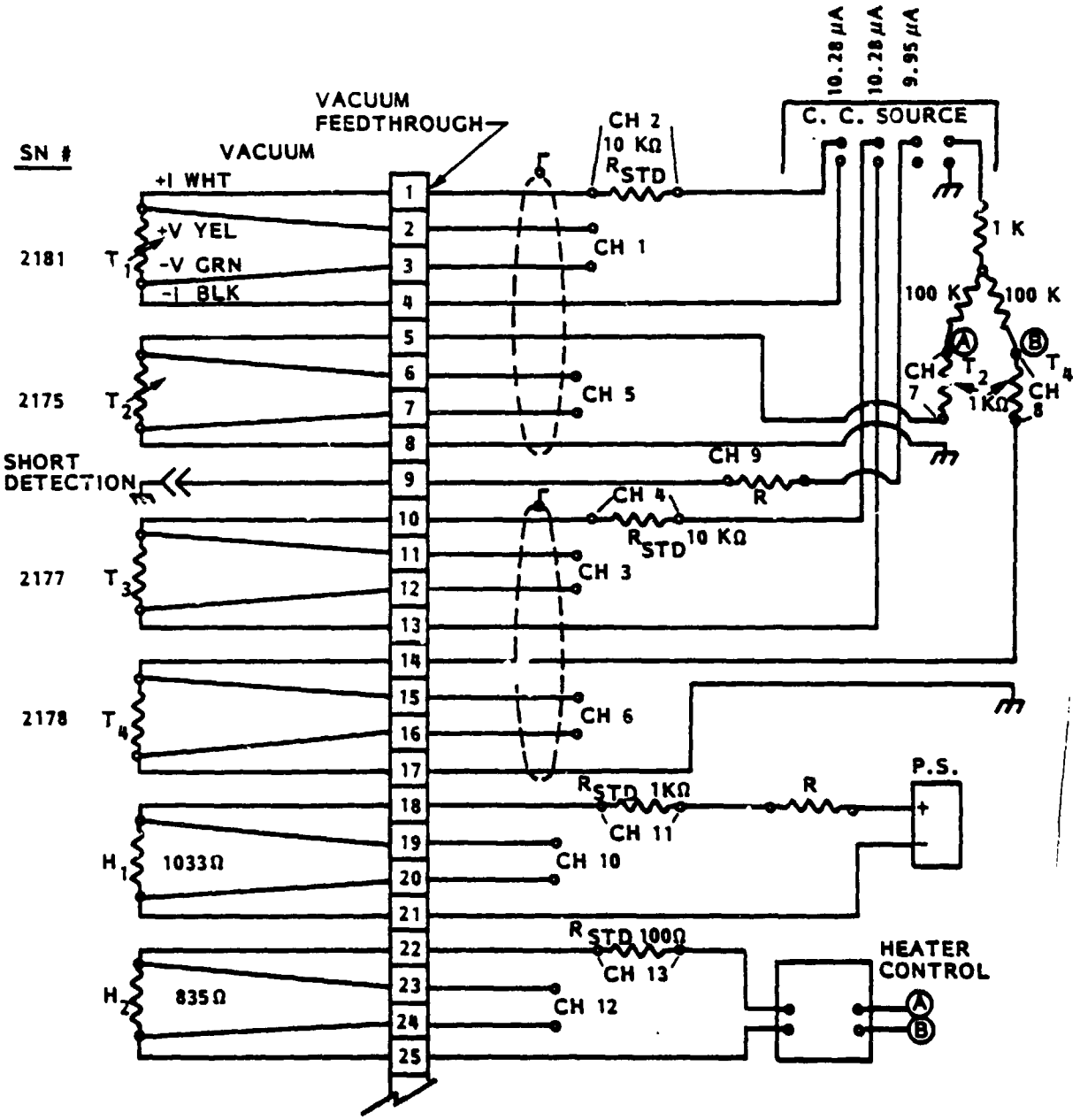

Fig. 29 Thermal Test Electrical Schematic

Table 6 TEST INSTRUMENTATION

Function		Instrumentation	CALIBRATED RANGE AGAINST NBS STANDARD
T_1	Measure helium heat sink temperature (S/N 2181)	Cryocal Model CC-1000-CA-VM-1%-GENAB Carbon Composition Resistance Thermometer, four 3 mil chromel lead wires, constant current source. Precision resistance shunt in series with thermometer leg to measure current.	4-20K*
T_2	Measure the warm side temperature of the thermal link (S/N 2175).		4-20K
T_3	Measure the test article body temperature (S/N 2177).		4-40K
T_4	Provides a signal for controlling heater H_2 (S/N 2178).		4-40K
H_1	Heater for thermal link calibration tests	1033-ohm heater, 4 each 3-mil chromel lead wires, resistor epoxy bonded into stem hole.	0 - 3 mW
H_2	Heater for simulated ground hold and orbit tests.	835-ohm heater, attached to body with acrylic adhesive, 4 each 3-mil chromel lead wires.	0 - 3 mW

*Resistance versus temperature printed out at 0.01-K increments.

Heater H_1 is used during thermal link calibration tests only. The controls for heater H_2 were designed to maintain temperature T_4 equal to T_2 during the thermal link calibration. However, this feature was not used, as explained later in the test results. Consequently, H_2 was only used to maintain the body at various temperature levels during the simulated ground hold and orbit tests. The test data were printed out on 13 channels at preset intervals using a Fluke 2240 C Datalogger.

Channel	Reduced Data
1. E across T_1	R_{T_1}
2. E across 10 K standard resistor in T_1 circuit	I_{T_1}
3. E across T_3	R_{T_3}
4. E across 10 K standard resistor in T_3 circuit	I_{T_3}
5. E across T_2	R_{T_2}
6. E across T_4	R_{T_4}
7. E across 999.7 standard resistor in T_2 circuit	I_{T_2}
8. E across 999.7 standard resistor in T_4 circuit	I_{T_4}
9. "Short" detector	Short or No short
10. E across H_1	R_{H_1}
11. E across 1 K standard resistor in H_1 circuit	I_{H_1}
12. E across H_2	R_{H_2}
13. E across 100 standard resistor in H_2 circuit	I_{H_2}

Where I = current
E = voltage
R = resistance

6.2 TEST PROCEDURE

6.2.1 Calibration Test

The space between the helium tank and LN_2 guard is evacuated to $<10^{-5}$ torr and the outer guard is filled with liquid nitrogen. An automatic resupply system tops off the guard every two hours. Once the helium tank has cooled to near liquid nitrogen temperature, the tank is filled with liquid helium. Temperature T_1 through T_4 are monitored until they reach equilibrium. When T_2, T_3, and T_4 would not cool down to T_1 (the heat sink), an investigation was undertaken to determine the cause.

Theory No. 1

The top of the copper tank is warm radiating to the test article through the four-layer MLI blanket. This theory is incorrect because the T_2–T_1 delta remained at 0.2 K whether the tank was just filled with liquid helium or was nearly empty.

Theory No. 2

The I^2R heating from T_2, T_3, and T_4 maintained the ΔT. This theory was also proven incorrect. The calculated I^2R heating for these three resistors is 1.1×10^{-4} mW, not nearly enough to maintain a 0.2-K delta between T_2 and T_1. To verify this, power was turned off to all temperature sensors and only turned on at 1-hour intervals over a six-hour period. The 0.2-K delta remained between T_2 and T_1.

Theory No. 3

Parasitic heat leaks from 21 3-mil chromel wire leads supply the heat. This is incorrect, because the 0.6-m long leads are thermally grounded to the copper plate at 4.3 K before they exit the vacuum system. Consequently, any

heat leaks would tend to equilibrate temperatures T_2, T_3, and T_4 with T_1, and not keep them elevated. Also, the calculated parasitic heat load through the wires is extremely low, $< 4 \times 10^{-6}$ mW.

Theory No. 4

The helium tank is leaking into the vacuum space. This theory is incorrect for two reasons. The vacuum pressure never got higher than 10^{-7} torr, and a leak would tend to drive temperatures T_2, T_3, and T_4 towards T_1 rather than keeping them elevated.

Theory No. 5

Vibrational energy from the vacuum pumping system is being transmitted to the test article through the pumping line. A definite high-frequency resonance can be felt on the top of the dewar. If, for example, it is assumed that the test article body is vibrating at 10 Hz, it only takes a lateral movement of 0.001 mm in the fiberglass tube to deposit the 0.05-mW heat rate into the system that is being measured. Since no other heat sources have been postulated, this seems to be the most likely cause.

To obtain a calibration point, heater H_1 is turned on. Once temperature equilibrium is achieved, a new H_1 power level is set, and the test is repeated. (Temperature equilibrium is defined as a change of less than 0.01 K over a period of 8 hours.) Enough data points are obtained so a ΔT ($T_2 - T_1$) versus power curve (H_1) is plotted up to 3 mW.

6.2.2 Simulated Ground Hold and Orbit Tests

Heater H_2 is turned on. (Heater H_1 is off for these tests.) The body temperature T_4 is raised and stabilized near 10 K. Once temperature equilibrium is achieved for 8 hours, T_4 is raised to 20 K, then 30 K and finally 40 K. (Temperature equilibrium is defined as a change of less than 0.01 degrees K over a period of 8 hours.)

For the measured ΔT ($T_2 - T_1$), the heat leak is obtained from the previously measured thermal link calibration curve. (Note: The heater power (H_2) versus ΔT ($T_2 - T_1$) curve should be nearly identical with the calibration curve. The test data provided later in Section 6.3 show that this is indeed the case.) The measured heat rates (H_2 power plus vibration correction) are then compared to the predicted values over the temperature range of 10 to 40 K using the equation from Section 3.3.

6.3 TEST RESULTS

The test data for equilibrium temperatures prior to and following the tests (1, 2), calibration runs (3-5), and test data points (6-9) are provided in Table 7.

Table 7 THERMAL TEST DATA

Test No.	T_2 (K)	T_1 (K)	$T_2 - T_1$ (K)	T_3 (K)	T_4 (K)	$\frac{T_3 + T_4}{2}$ (K)	$\frac{T_3 + T_4}{2} - T_2$ (K)	Heater Power (mW)	Vibration Correction (mW)	Total Heat Leak (mW)
1. Prior to Tests	4.76	4.54	0.216	6.06	6.09	6.08	1.32	0		
2. Following Tests	4.73	4.54	0.19	5.96	5.99	5.98	1.25	0	0.054	0.054
3. Calibration	5.33	4.55	0.78	7.01	7.05	7.03	1.70	0.4027	0.054	0.457
4. Calibration	6.23	4.58	1.65	8.51	8.57	8.54	2.31	1.1116	0.054	1.166
5. Calibration	7.24	4.60	2.64	10.19	10.29	10.24	3.00	2.108	0.054	2.162
6. Test	5.08	4.55	0.53	10.67	10.76	10.72	5.64	0.2052	0.054	0.259
7. Test	5.94	4.58	1.36	21.14	21.59	21.37	15.43	0.8367	0.054	0.891
8. Test	6.66	4.59	2.07	30.23	31.42	30.83	24.17	1.497	0.054	1.551
9. Test	7.27	4.63	2.64	38.04	39.70	38.87	31.60	2.139	0.054	2.193

The vacuum pressure remained in the 3×10^{-8} to 1×10^{-7} torr range during the tests. The heater power (H_1 or H_2) is plotted as a function of the ΔT across the thermal link ($T_2 - T_1$) in Fig. 30.

Note the good agreement between the calibration points and the test runs. This indicates that all the heat is flowing through the thermal link with negligible radiation loss to the helium tank or conduction loss along wires,

etc. Secondly, note that the ΔT does not go to zero at zero heater power. This heat input is assumed to be in the form of vibrational energy from the pumping system as discussed earlier in Section 6.2.1. Based on the average 0.20 K ΔT value for no heater power, the heat rate is 0.054 mW using the thermal model described in Section 3.3.

Figure 31 plots the measured heat leak through the PODS-III support as a function of the average body temperature, $(T_3 + T_4)/2$.

6.4 DISCUSSION OF TEST RESULTS

6.4.1 Comparison of Predicted and Measured Heat Rates

Using the thermal model described in Section 3.3, the measured heat rates were compared with the predicted values as shown in Table 8 and Fig. 32.

Table 8 MEASURED VERSUS PREDICTED HEAT RATES

Temperatures (K)		Heat Leak		
T_2	$\frac{T_3 + T_4}{2}$	Measured mW	Predicted** mW	Percent Difference
4.75	6.03	0.054*	0.054	-
5.08	10.72	0.259	0.289	10
5.94	21.37	0.891	1.009	12
6.66	30.83	1.551	1.826	15
7.27	38.87	2.193	2.604	16

*Calculated value based on measured temperatures.
**Calculated value based on measured temperatures; includes epoxy thickness variation effect.

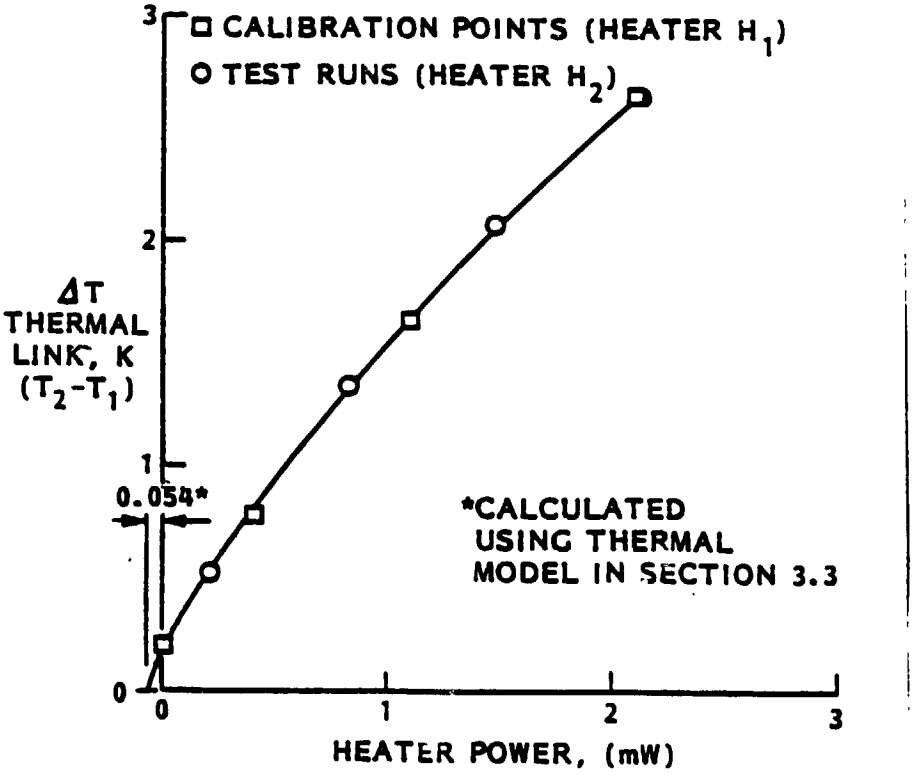

Fig. 30 Thermal Link Calibration Data Versus Test Data

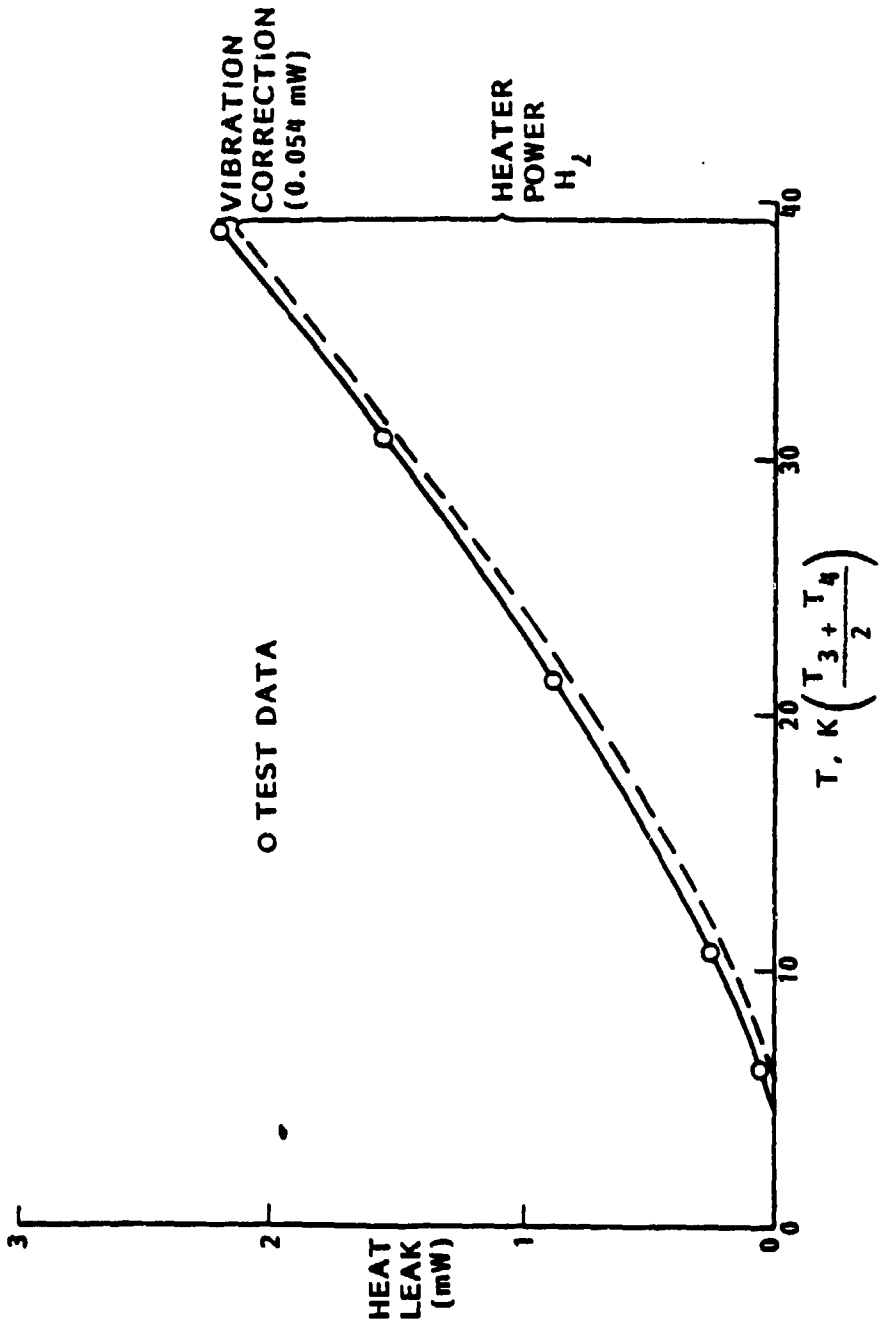

Fig. 31 Measured Heat Rates

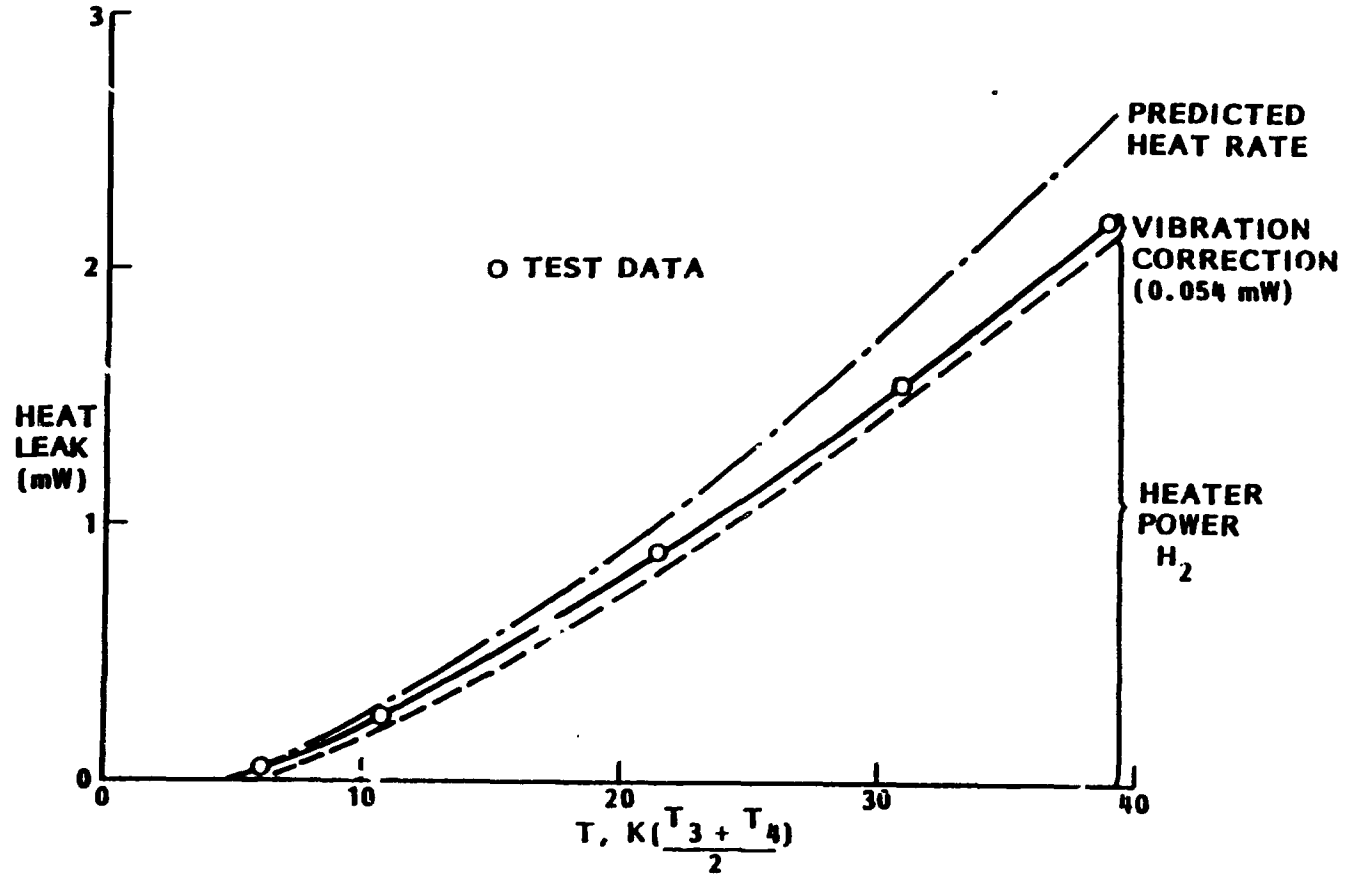

Fig. 32 Measured Versus Predicted Heat Rates

Note that the predicted heat rates are 10 to 16 percent higher than the measured heat rates for equivalent warm and cold boundary temperatures. An analysis was performed to see if the variations in cross sectional area could account for the predicted values being higher than the measured values. (Note: The fiberglass/epoxy tube has a wavy outer surface due to the winding pattern. It was noted previously in Section 4.1 that the average wall thickness of the tube, 0.345 mm, as determined by a water immersion test is less than the maximum wall thickness as determined by a direct measurement, 0.381 mm.)

These thickness variations are only in the epoxy matrix since the number and consequently the cross sectional area of the fiberglass filaments remain constant.

The variation in epoxy thickness was estimated as follows.

$$\text{Normalized Epoxy Thickness Variation} = \frac{(\text{Max. Total Wall Thickness}) - (\text{Ave. Total Wall Thickness})}{(\text{Volume Fraction of Epoxy})\ (\text{Ave. Total Wall Thickness})}$$

$$= \frac{(0.381 - 0.345)}{(0.364)\ (0.345)} = 0.287$$

This thickness variation down the tube reduces the heat rate through the epoxy (or increases the epoxy resistance) by 8.8 percent as shown in Fig. 33. (Appendix A provides the derivation of this curve.)

When the epoxy resistance in the tube was increased 8.8 percent using the thermal model from Section 3.3, the overall heat rate only decreased between 0.9 to 1.2 percent. (Predicted values in Table 8 include this correction.)

Consequently, thickness variation can only account for a small fraction of the difference between the predicted and measured heat rates.

Other items that may account for the differences are: (1) the uncertainities in the test data values as discussed later in Section 5.4.2; (2) the accuracy

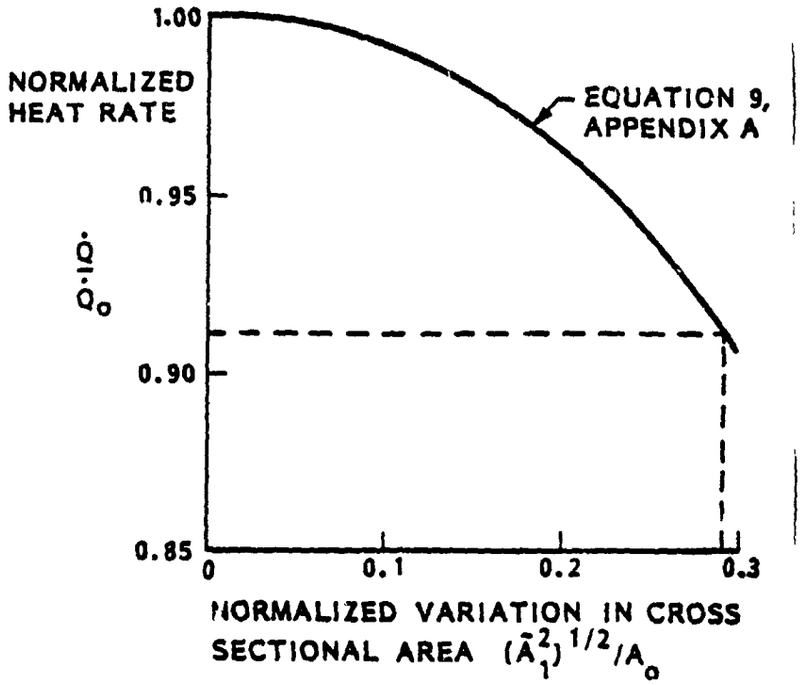

Fig. 33 Effect of Variations in Cross Sectional Area on Epoxy Heat Rates in the Fiberglass Tube

of the thermal conductivity values taken from the literature and used in the analyses; and (3) the contact resistance of the gold coated Invar threads at the adjustment bushing/body connection and the gold coated Invar stem/stainless steel rod-end (thermal link) attachment. In any event, the predicted heat rates provide a suitable design margin over measured values (10 to 16 percent) and are recommended for use in future heat rate calculations.

6.4.2 Experimental Uncertainties

The uncertainties in the measured temperatures and heat rates are provided in Table 9. Note that the carbon temperature sensors accuracy is good below 10 K but gets progressively worse up to 40 K. This uncertainty was obtained by comparing temperature T_3 to temperature T_4. The maximum uncertainty in the heat rate is expressed as the sum (not the lower RMS value) of uncertainties in the vibration correction, power supply stability, parasitic heat loss down the wires, and I^2R heating of the temperature sensors. Note that the vibration correction is the dominant uncertainty.

Table 9 UNCERTAINTY IN TEST DATA

Test No.	T_2 (K)	T_3, T_4 (K)	H_2 + Vibration Correction (mW)
1, 2	4.75 ± 0.01	6.03 ± 0.02	0.054 ± 0.020*
6	5.08 ± 0.01	10.72 ± 0.04	0.25 ± 0.021
7	5.94 ± 0.02	21.37 ± 0.23	0.89 ± 0.022
8	6.66 ± 0.02	30.83 ± 0.53	1.55 ± 0.023
9	7.27 ± 0.02	38.87 ± 0.74	2.19 ± 0.025

	Test No.				
	1,2	6	7	8	9
• Vibration Correction (mW)	0.02	0.02	0.02	0.02	0.02
• Power Supply Stability (mW)	–	0.0006	0.0019	0.0032	0.0045
• Parasitic Heat Loss Down 25 Chromel Wires (mW)	$< 4 \times 10^{-6}$	$< 4 \times 10^{-6}$	$< 4 \times 10^{-6}$	$< 4 \times 10^{-6}$	$< 4 \times 10^{-6}$
• I^2R Heating of T_1, T_2, T_3, T_4 (mW)	0.00020	0.00016	0.00014	0.00013	0.00013
TOTAL* (mW)	0.020	0.021	0.022	0.023	0.025

Section 7
PODS-III STRUCTURAL AND THERMAL PERFORMANCE DATA SUMMARY

As a convenience to the reader, measured PODS-III thermal and structural performance data are summarized here.

Weight, g(lb)	
• Adjustment Bushing	19.1
• Fiberglass Tube	1.9
• Stem	33.6
• Clamshells (4 ea)	3.7
• Nut	59.8
• Body (Full Undercut - not Made)	150.0
• Rod End	42.7
	311 (0.69)

Load Direction	Recommended Gaps (mm (in.))		
	290 K		2 K
	Axial	Shim Thickness	Axial
Tension	0.58 (0.0023)	0.51 (0.002)	0.099 (0.0039)
Compression	0.140 (0.0055)	0.122 (0.0048)	0.099 (0.0039)

Measured Shorting Loads, N (lb_f) Shim Thickness = 0.076 mm (0.003 in.)		
Load Direction	290 K	2 K (Calculated)
Axial Tension Axial Compression Radial (Side)	609 (136.9) 524 (117.8) 11.1 (2.49)	914 (205) 796 (179) 16.7 (3.24)

Heat Leak (mW)				
Flight Phase	$T_{VACSHELL}$ (K)	T_{BODY} (K)	T_C (K)	mW
• Ground Hold	290	4.2	2	0.05
• Orbit	200	15.3	2	0.6

Section 8
CONCLUSIONS AND RECOMMENDATIONS

The following conclusions and recommendations can be reached on the PODS-III concept based on the results of the development program to date.

- The thermal performance of PODS-III is equal to or better than prior predictions.

- Use the thermal model for future predictions (to provide a design margin of 10 to 16 percent).

- The nonshorting feature of the design works, although the assembly procedure requires modification to keep the stem properly centered during epoxy bonding. (Section 5 includes the corrected procedure.)

- Offset the axial gap spacing of 0.041 mm (0.0016 in.) to account for the differential thermal contraction between the fiberglass tube and Invar parts at LHe temperature.

- Perform side load and axial compression and tension load tests per Section 4.5 as a quality check on the assembly procedure.

- Interweave the filament wound fiberglass tube (HE0014) every 0.8 cm (0.4 in.) as called out in Fig. 8 to improve ultimate compression strength. The ± 30 deg tubes that were tested were interwoven every 2 to 4 cm (0.8 to 1.6 in.).

Section 9
REFERENCES

1. Parmley, R. T., Feasibility Study for Long Lifetime Helium Dewar, NASA-CR166254, Dec 1981.

2. Radcliffe, D. J. and Rosenburg, H. M., "The Thermal Conductivity of Glass-Fibre and Carbon-Fibre/Epoxy Composites from 2 to 80K," Cryogenics, May 1982, p. 245.

3. Hust, J. G. and Arvidson, J. M., Thermal Conductivity of Glass Fiber/Epoxy Composite Support Bands for Cryogenic Dewars, NBS Report 275.03-78-2, Feb 1978.

4. Childs, G. E. et al., Thermal Conductivity of Solids at Room Temperature and Below, NBS Mongraph 131, Sep 1973, p. 257.

5. Compendium of Thermophysical Properties, WADD TR60-56 Part II, Aug 1960, p. 3.301.

6. Kasen, M. B., "Cryogenic Properties of Filamentary-Reinforced Composites: An Update," Cryogenics Jun 1981, pp. 323-340.

7. "Materials-Key Decision in Low Temperature Piping," Design, Heating, Piping and Air Conditioning, Sep 1965, p. 154.

8. Campbell, M. D., "Thermal Expansion Characteristics of Some Plastic Materials and Composites from Room Temperature to -253°C," (paper presented at Cryogenic Engineering Conference, Philadelphia, Aug 1964).

Appendix A
EFFECT OF VARIATION OF CROSS-SECTIONAL AREA ON THE THERMAL CONDUCTANCE OF THE FIBERGLASS/EPOXY TUBE

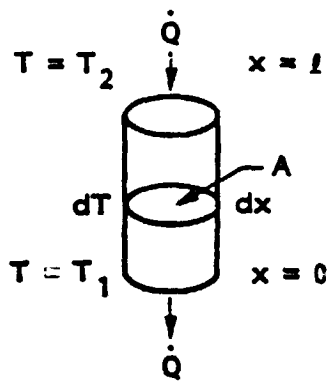

The governing equation is

$$\dot{Q} = \quad JT/dx \tag{1}$$

for the case of constant cross section ($A = A_0$). This reduces to:

$$\dot{Q}_0 \frac{\ell}{A_0} = \int_{T_1}^{T_2} k(T)\, dT \tag{2}$$

For a nonconstant A, we can separate the variables in (1)

$$\dot{Q} \int_0^L \frac{dx}{A(x)} = \int_{T_1}^{T_2} k(T)\, dT \tag{3}$$

or by (2)

$$\dot{Q}\int_0^L \frac{dx}{A(x)} = \dot{Q}_0 \frac{\ell}{A_0} \tag{4}$$

expand A: $A(x) = A_0 + A_1(x)$ where:

$$\begin{cases} \bar{A}(x) = A_0 \\ \bar{A}_1(x) = 0 \end{cases}$$

($\bar{z}$ means average of z over x, i.e., $\bar{z} = \frac{1}{L}\int_0^L z\, dx$)

Eq. 4 becomes

$$\dot{Q}\int_0^L \frac{dx}{A_0 + A_1(x)} = \dot{Q}\ \frac{\ell}{A_0} \tag{5}$$

Expand the integral of (5) keeping only the lowest order terms.

$$\frac{\dot{Q}}{A_0}\int_0^L \left[1 - \frac{A_1}{A_0} + \frac{A_1^3}{A_0^2} - \ldots\right] dx = \frac{\dot{Q}_0 L}{A_0} \tag{6}$$

Integrate and multiply both sides by A_0/L, recall $\bar{A}_1 \equiv 0$

$$\dot{Q}\left[1 + \frac{A_1^2}{A_0^2}\right] = \dot{Q}_0 \tag{7}$$

including higher order terms:

$$\dot{Q}\left[1 + \sum_{n=2}^{\infty}(-1)^n \frac{A_1^n}{A_o^n}\right] = \dot{Q}_o \tag{8}$$

If the probability of a particular value $\bar{A}_1$ occuring equals that of a negative A_1 occuring, then the odd powers drop out of (8) and

$$\dot{Q}\sum_{n=0}^{\infty}\left[\bar{A}_1^{2n}/A_o^{2n}\right] = \dot{Q}_o \tag{9}$$

where

A = cross sectional area of tube

A_o = cross sectional area of tube with constant wall thickness

k = thermal conductivity

ℓ = length

$\dot{Q}$ = heat rate

$\dot{Q}_o$ = heat rate of tube with constant cross sectional area

T = absolute temperature